Journal Name

Crossmark

RECEIVED
dd Month yyyy

REVISED
dd Month yyyy

PAPER Response of a magnetically diverted tokamak plasma to a resonant magnetic perturbation

Richard Fitzpatrick Institute for Fusion Studies, Department of Physics, University of Texas at Austin, Austin TX 78712, USA **E-mail:** rfitzp@utexas.edu

Abstract

The safety-factor profile of a magnetically diverted tokamak plasma diverges logarithmically as the magnetic separatrix (a.k.a. the last closed magnetic flux-surface) is approached. At first sight, this suggests that, when determining the response of such a plasma to a static, externally generated, resonant magnetic perturbation (RMP), it is necessary to include an infinite number of rational magnetic flux-surfaces (at which the RMP resonates with the equilibrium magnetic field) in the calculation, the majority of which lie very close to the separatrix. In fact, when finite plasma resistivity is taken into account, this turns out not to be the case. Instead, it is only necessary to include rational surfaces that lie in the region $0 < \Psi < 1 - \epsilon_c$, where Ψ is the normalized poloidal magnetic flux, and $0 < \epsilon_c \ll 1$. The parameter ϵ_c can be calculated from the edge plasma parameters.

1 Introduction

All modern tokamak plasmas feature a *magnetic divertor*, which is a particular configuration of the magnetic field that redirects the outermost field-lines away from the confined plasma region and into a controlled exhaust area where the plasma particle and heat fluxes can be safely absorbed by a solid target plate [1]. Each magnetic flux-surface in a tokamak plasma has an associated value of the *safety-factor*, which specifies the number of toroidal circuits of the surface that a constituent magnetic field-line makes per poloidal circuit [2, 3]. Magnetic flux-surfaces possessing rational values of the safety-factor are special. Indeed, externally generated, static, non-axisymmetric magnetic perturbations—known as *resonant magnetic perturbations* (RMPs)—can drive magnetic reconnection on such *rational surfaces*, leading to localized changes in magnetic topology that degrade the ability of the surrounding flux-surfaces to confine energy [4]. Alternatively, shielding currents can flow, predominately parallel to magnetic field-lines, on rational surfaces, and act to suppress driven magnetic reconnection [5]. In general, neither driven magnetic reconnection nor shielding currents can occur on irrational magnetic flux-surfaces.

A magnetically diverted tokamak plasma possesses a so-called "last closed magnetic flux-surface" (LCFS). Magnetic flux-surfaces that lie inside the LCFS are topologically simple tori, and are completely occupied by plasma. Magnetic flux-surfaces that lie outside the LCFS have more complicated topology, and are only partially occupied by plasma. The LCFS features a magnetic "X-point", which is a circular loop, coaxial with the plasma torus, on which the poloidal magnetic field is zero. (In some very special tokamak plasmas, the LCFS features two X-points. However, we shall not consider such plasmas here.) As the LCFS is approached, the safety-factor exhibits a logarithmic singularity [6], as a direct consequence of the presence of the X-point, and there is an associated accumulation of rational magnetic flux-surfaces in the vicinity of the LCFS. In fact, for an RMP with a given toroidal mode number, there are, in principle, an *infinite* number of associated rational surfaces, most of which lie very close to the LCFS, on which the RMP can drive magnetic reconnection. It is impossible to include all of these surfaces in a practical plasma response calculation. Hence, the standard approach is to simply ignore rational flux-surfaces associated with very high values of the safety-factor [8, 9, 10, 11, 12, 13, 14]. The purpose of this paper is to investigate to what extent this approach is justified.

This paper is organized as follows. A particularly simple model of a magnetically diverted tokamak plasma is introduced in Sect. 2, and is used to define exactly what is meant by a straight-field-line coordinate system, the safety-factor profile, and a rational surface, both inside and outside the LCFS. A more realistic model of a magnetically diverted tokamak plasma is presented in Sect. 3. The response of a magnetically diverted plasma to an RMP is analyzed in

Sect. 4. Section 5 investigates the predictions of the plasma response model in the vicinity of the LCFS. Finally, the paper is summarized in Sect. 6.

2 Simple model of a magnetically diverted plasma

The aim of Sect. 2 is to construct a very simple model of a magnetically diverted tokamak plasma.

2.1 Equilibrium magnetic field

Let x, y, z be conventional Cartesian coordinates. Suppose that two current filaments run parallel to the z-axis [6, 7]. Let the first filament carry the current I_p, and pierce the x-y plane at $x = y = 0$. Let the second filament carry the current I_c, and pierce the x-y plane at $x = 0$, $y = -a$. The first filament represents the "toroidal" (i.e., z-directed) plasma current, whereas the second represents the toroidal current flowing in the magnetic divertor coil that generates the magnetic X-point. Suppose that there is a uniform, externally generated, toroidal magnetic field of strength B_0. Let the system be periodic in the z-direction with period $2\pi\,R_0$, where R_0 is the simulated major radius of the plasma. It is helpful to define the simulated toroidal angle, $\phi = z/R_0$.

The equilibrium magnetic field can be written in the divergence-free manner

$$\mathbf{B} = \nabla\phi \times \nabla\psi_p + B_0\,R_0\,\nabla\phi, \tag{1}$$

where

$$\psi_p(x,y) = \frac{\mu_0\,I_p\,R_0}{4\pi}\,\ln\left(x^2+y^2\right) + \frac{\mu_0\,I_c\,R_0}{4\pi}\,\ln\left[x^2+(y+a)^2\right] \tag{2}$$

is the "poloidal" (i.e., circulating in the x-y plane) magnetic flux (divided by 2π) generated by the two current filaments.

2.2 Straight-field-line coordinates

It is convenient to re-express the magnetic field in the standard Clebsch form

$$\mathbf{B} = \nabla(\phi - q\,\theta) \times \nabla\psi_p, \tag{3}$$

where θ is a poloidal angle, and $q = q(\psi_p)$ the (dimensionless) *safety-factor* [15]. Equations (1) and (3) can be reconciled provided

$$\nabla\psi_p \times \nabla\theta \cdot \nabla\phi = \frac{B_0}{R_0\,q}. \tag{4}$$

Note, from Eq. (3), that $\mathbf{B}\cdot\nabla\psi_p = 0$, which implies that ψ_p is a magnetic flux-surface label. Furthermore, $\mathbf{B}\cdot\nabla(\phi - q\,\theta) = 0$, which implies that magnetic field-lines within a given flux-surface appear as straight lines, with gradient $d\phi/d\theta = q$, when plotted in the θ-ϕ plane. In fact, ψ_p, θ, ϕ are known as *straight-field-line coordinates*, and θ is termed a *straight* poloidal angle [15]. The defining property of a straight-field-line coordinate system is the choice $q = q(\psi_p)$, rather than $q = q(\psi_p,\theta)$, or even $q = q(\psi_p,\theta,\phi)$. There are many types of straight-field-line coordinate systems (e.g., Hamada [16], Boozer [17], PEST [18], equal-arc), all of which have the required property that $q = q(\psi_p)$. For the sake of convenience, in this paper we shall adopt PEST coordinates, which are characterized by a toroidal angle, ϕ, that corresponds to the angular coordinate in the R, ϕ, Z cylindrical coordinate system (that is coaxial with the plasma torus). (Here, we are looking ahead to the generalization to true toroidal geometry that takes place in Sect. 3.1.) Once the choice of toroidal angle is made, the straight-field-line coordinate system is uniquely defined.

2.3 Non-diverted edge safety-factor

In the absence of the divertor current, the plasma would have a circular cross-section in the x-y plane of minor radius a, and an edge safety-factor value of

$$q_* = \frac{2\pi\,B_0\,a^2}{\mu_0\,I_p\,R_0}. \tag{5}$$

2.4 Normalization scheme

Let $x = a\,X$, $y = a\,Y$, $\nabla = a^{-1}\,\hat{\nabla}$, and $\psi_p = \mu_0\,I_p\,R_0\,\psi/(2\pi)$. It follows that

$$\hat{\nabla}\psi \times \hat{\nabla}\theta \cdot \hat{\nabla}\phi = \frac{a}{R_0}\,\frac{q_*}{q}, \tag{6}$$

$$\psi(X,Y) = \frac{1}{2}\,\ln\left(X^2+Y^2\right) + \frac{\zeta}{2}\,\ln\left[X^2+(Y+1)^2\right], \tag{7}$$

$$\psi_X(X,Y) = \frac{X}{X^2+Y^2} + \frac{\zeta\, X}{X^2+(Y+1)^2}, \tag{8}$$

$$\psi_Y(X,Y) = \frac{Y}{X^2+Y^2} + \frac{\zeta\,(Y+1)}{X^2+(Y+1)^2}, \tag{9}$$

where $\zeta = I_c/I_p$. Here, $\psi_X \equiv \partial\psi/\partial X$, et cetera.

2.5 Magnetic X-point

The magnetic X-point is located at the point in the X-Y plane where $\psi_X = \psi_Y = 0$ (i.e., where the poloidal magnetic field-strength is zero). As is easily demonstrated, the coordinates of this point are (X_x, Y_x), where $X_x = 0$ and $Y_x = -1/(1+\zeta)$. The so-called magnetic separatrix corresponds to the curve $\psi(X,Y) = \psi_x$, where

$$\psi_x \equiv \psi(X_x, Y_x) = \ln\left[\frac{\zeta^\zeta}{(1+\zeta)^{1+\zeta}}\right]. \tag{10}$$

It is helpful to define the normalized poloidal flux, $\Psi = \psi_x/\psi$. (Note that this definition is different from the conventional one, $\Psi = \psi/\psi_x$, because $\psi \to \infty$ on the magnetic axis, $X = Y = 0$, and we wish the normalized flux to increase as we go from the axis to the separatrix.)

2.6 Construction of straight-field-line coordinate system

A unit vector that runs around a magnetic flux-surface in the X-Y plane in the direction of increasing θ is such that

$$\mathbf{n} = \frac{\hat{\nabla}\phi \times \hat{\nabla}\psi}{|\hat{\nabla}\phi|\,|\hat{\nabla}\psi|} \tag{11}$$

because $\mathbf{n}\cdot\hat{\nabla}\psi = 0$ within a magnetic flux-surface, $\mathbf{n}\cdot\hat{\nabla}\phi = 0$ for a path confined to the X-Y plane, and $\hat{\nabla}\phi\cdot\hat{\nabla}\psi = 0$. Thus, Eq. (6) yields

$$\frac{d\theta}{dL} \equiv \mathbf{n}\cdot\hat{\nabla}\theta = \frac{q_*}{q\,|\hat{\nabla}\psi|} \tag{12}$$

where dL is an element of normalized length (in the X-Y plane) around the flux-surface, and use has been made of $|\hat{\nabla}\phi| = a/R_0$. It follows that

$$q(\psi) = \frac{q_*}{2\pi}\oint \frac{dL}{|\hat{\nabla}\psi|}, \tag{13}$$

where $\oint$ implies a complete circuit in θ at constant ψ. It is easily demonstrated that, on such a circuit,

$$\frac{dX}{dL} = -\frac{\psi_Y}{\sqrt{\psi_X^2+\psi_Y^2}}, \tag{14}$$

$$\frac{dY}{dL} = \frac{\psi_X}{\sqrt{\psi_X^2+\psi_Y^2}}, \tag{15}$$

$$\frac{d\phi}{dL} = \frac{q_*}{\sqrt{\psi_X^2+\psi_Y^2}}, \tag{16}$$

$$\frac{d\varpi}{dL} = \frac{X\,\psi_X + Y\,\psi_Y}{(X^2+Y^2)\sqrt{\psi_X^2+\psi_Y^2}}, \tag{17}$$

where

$$\varpi = \tan^{-1}\left(\frac{Y}{X}\right) \tag{18}$$

is a geometric poloidal angle. Here, ϕ is calculated on the assumption that we are following a magnetic field-line within the flux-surface (i.e., $d\phi/d\theta = q$). We need to integrate Eqs. (14)–(17) from $\varpi = 0$ to $\varpi = 2\pi$, subject to the initial condition $\phi(\varpi = 0) = 0$, and then set $q(\psi) = \phi(\varpi = 2\pi)/(2\pi)$. We can then compute θ using

$$\frac{d\theta}{dL} = \frac{q_*}{q\sqrt{\psi_X^2+\psi_Y^2}}. \tag{19}$$

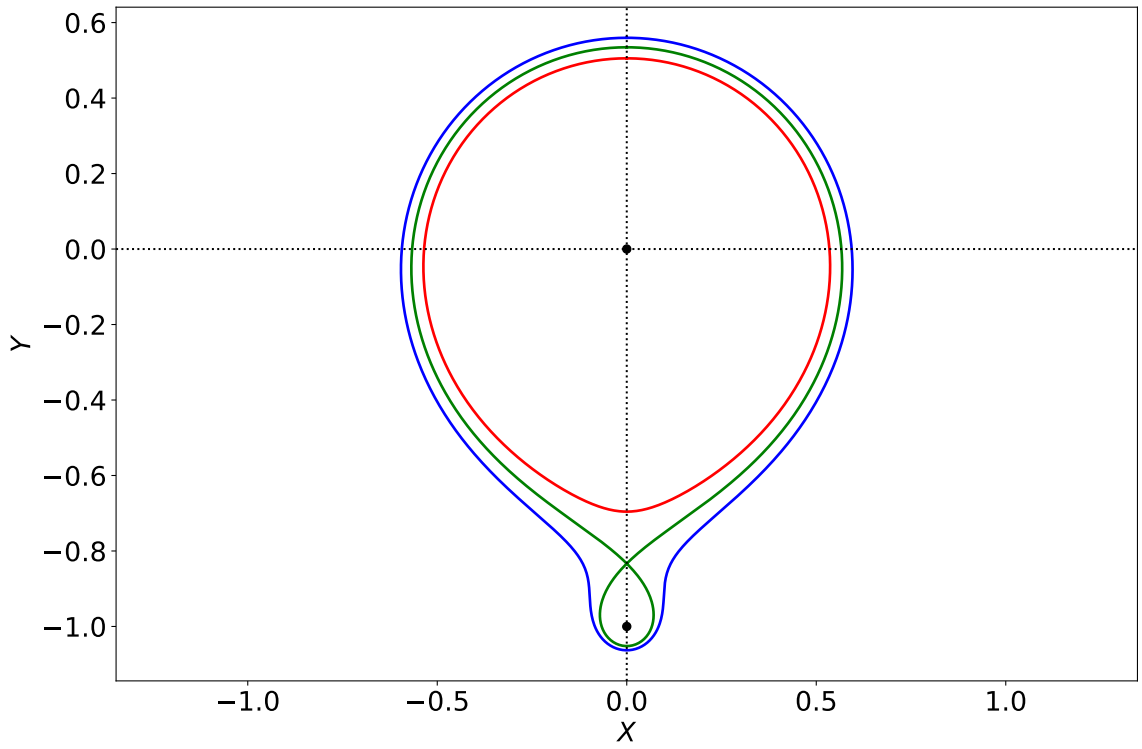

Figure 1. The magnetic flux-surfaces $\Psi = 0.9$ (red), $\Psi = 1.0$ (green), and $\Psi = 1.1$ (blue) in the absence of a divertor plate. The black dots shows the locations of the two current filaments. Here, $q_* = 12$ and $\zeta = 0.2$.

Let $q_* = 12$ and $\zeta = 0.2$. Figure 1 shows the magnetic flux-surfaces $\Psi = 0.9$, $\Psi = 1.0$, and $\Psi = 1.1$, plotted in the X-Y plane. Flux-surfaces characterized by $\Psi < 1$ do not enclose the divertor coil filament, whereas those characterized by $\Psi > 1$ do enclose the filament. The *magnetic separatrix*, $\Psi = 1$, separates flux-surfaces that do and do not enclose the divertor coil filament, and crosses itself at the magnetic X-point.

The red and blue curves in Fig. 2 show the safety-factor profile, $q(\Psi)$, inside and outside the magnetic separatrix, respectively. It is clear that the safety-factor generally increases with increasing Ψ. However, $q \rightarrow \infty$ as $\Psi \rightarrow 1$. In other words, the safety-factor tends to infinity as the magnetic separatrix is approached from either direction. It is apparent from the bottom panel of Fig. 2 that q approaches infinity *logarithmically* as $\Psi \rightarrow 1$ (because the plot of q versus $\log_{10}(|\Psi - 1|)$ asymptotes to a straight line as $|\Psi - 1| \rightarrow 0$). In other words, close to the separatrix, we can write

$$q(\Psi) \simeq -\alpha_- \ln(1 - \Psi) \tag{20}$$

for $\Psi < 1$, and

$$q(\Psi) \simeq -\alpha_+ \ln(\Psi - 1) \tag{21}$$

for $\Psi > 1$. Moreover, the figure implies that $\alpha_+ > \alpha_-$. The reason that α_+ exceeds α_- is because magnetic field-lines lying in flux-surfaces situated just outside the X-point have an extra distance to travel to get around the flux-surface compared to those lying in flux-surfaces situated just within the X-point, which has the effect of increasing the integral (13). (This explanation is reinforced by the observation that when we introduce the divertor plate into the calculation, in Sect. 2.8, which has the effect of shortening the travel path of the former field-lines, then α_+ is reduced.)

Figures 3 and 4 show the straight-field-line coordinate system inside and outside the magnetic separatrix, respectively. It can be seen that, as the magnetic separatrix is crossed, all of the contours of θ converge onto, and then diverge away from, the X-point. This singular behavior occurs because $|\hat{\nabla}\psi| \rightarrow \ell$ and $|\hat{\nabla}\theta| \rightarrow 1/[\ell \ln|\Psi - 1|]$ as the X-point is approached, where ℓ represents distance from the X-point in the X-Y plane

2.7 Significance of straight-field-line coordinates

To understand the significance of the straight-field-line coordinate system, suppose that the plasma is subject to a static (in the laboratory frame) magnetic perturbation that varies with θ and ϕ as $\exp[\mathrm{i}\,(m\,\theta - n\,\phi)]$. Here, m and n are integers. In other words, the perturbation (which is, of

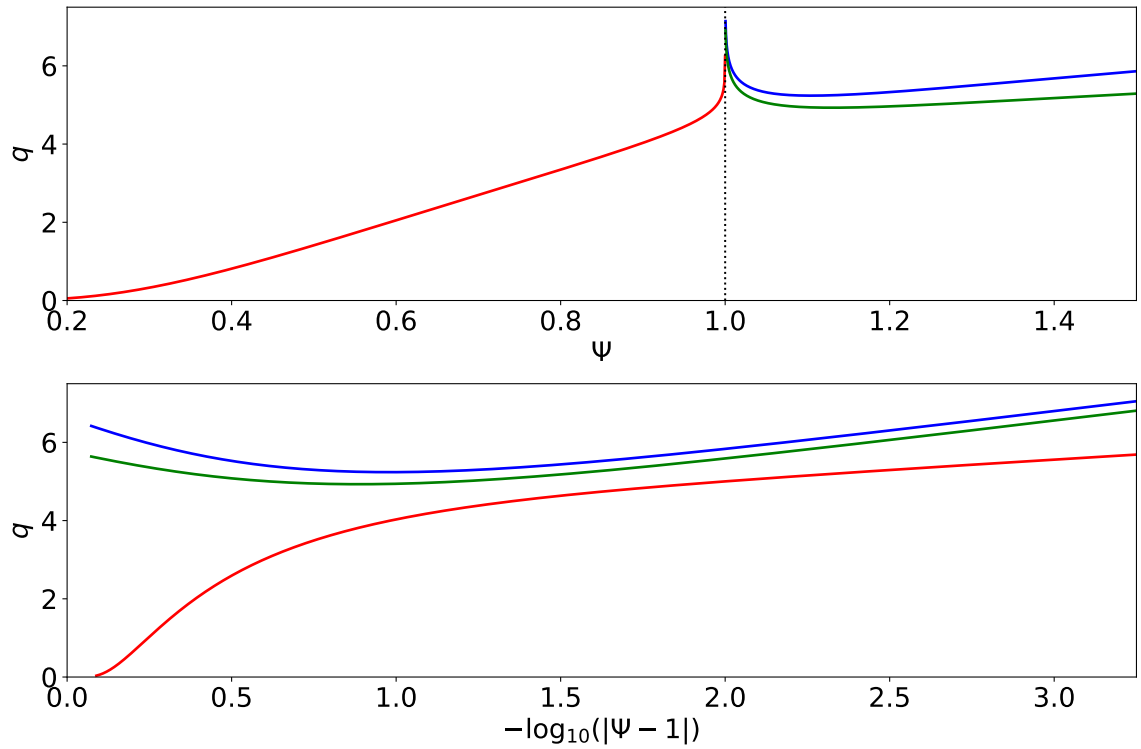

Figure 2. The safety-factor profile, $q(\Psi)$. The red curve shows the safety-factor inside the magnetic separatrix. The blue and green curves show the safety-factor outside the separatrix in the absence and in the presence of a divertor plate, respectively. Here, $q_* = 12$ and $\zeta = 0.2$.

course, single-valued in the angular coordinates θ and ϕ) possesses m periods in the poloidal angle, and n periods in the toroidal angle. The curl of the perturbed, linearized, electron fluid equation of motion yields (see Sect. A)

$$n\,(\omega_E + \omega_{*\,e})\left[b^{\psi_p} - \mathrm{i}\,\frac{B_0}{R_0}\left(\frac{m}{q} - n\right)\xi^{\psi_p}\right] \simeq \frac{B_0}{R_0}\,\frac{m}{q}\,\eta_\parallel\, j_\phi, \tag{22}$$

where subscripts and superscripts denote covariant and contravariant components in the ψ_p, θ, ϕ coordinate system, respectively [2]. Here, $\mathbf{b}$ is the perturbed magnetic field, $\boldsymbol{\xi}$ the Lagrangian electron fluid displacement, $\mathbf{j}$ the perturbed current density, and $\eta_\parallel$ the plasma parallel electrical resistivity. Moreover,

$$\omega_E(\psi_p) = -\frac{d\Phi}{d\psi_p} \tag{23}$$

is the *E-cross-B frequency*, whereas

$$\omega_{*\,e}(\psi_p) = \frac{1}{e\,n_e}\,\frac{dp_e}{d\psi_p} \tag{24}$$

is the *electron diamagnetic frequency*. Here, $\Phi(\psi_p)$ is the equilibrium electrostatic potential, $p_e(\psi_p)$ the equilibrium electron pressure, $n_e(\psi_p)$ the equilibrium electron number density, and e the magnitude of the electron charge.

Equation (22) describes how the inductive electric field generated by a time-varying magnetic field, as seen in rest frame of the local electron fluid, attempts to drive a current that runs parallel to magnetic field-lines. On a general magnetic flux-surface, the two terms (in the large square brackets) on the left-hand side of the equation cancel one another out, and there is no driven current. In other words, the electron fluid displaces rather than allowing a parallel inductive current to flow [5]. However, it is clear from the equation that there exists a special magnetic flux-surface, termed a *rational* flux-surface, at which the safety-factor takes the rational value $q = m/n$ [15]. On the rational flux-surface, the two terms on the left-hand side of Eq. (22) cannot cancel one another out, because the second term is zero everywhere on the surface. Hence, in

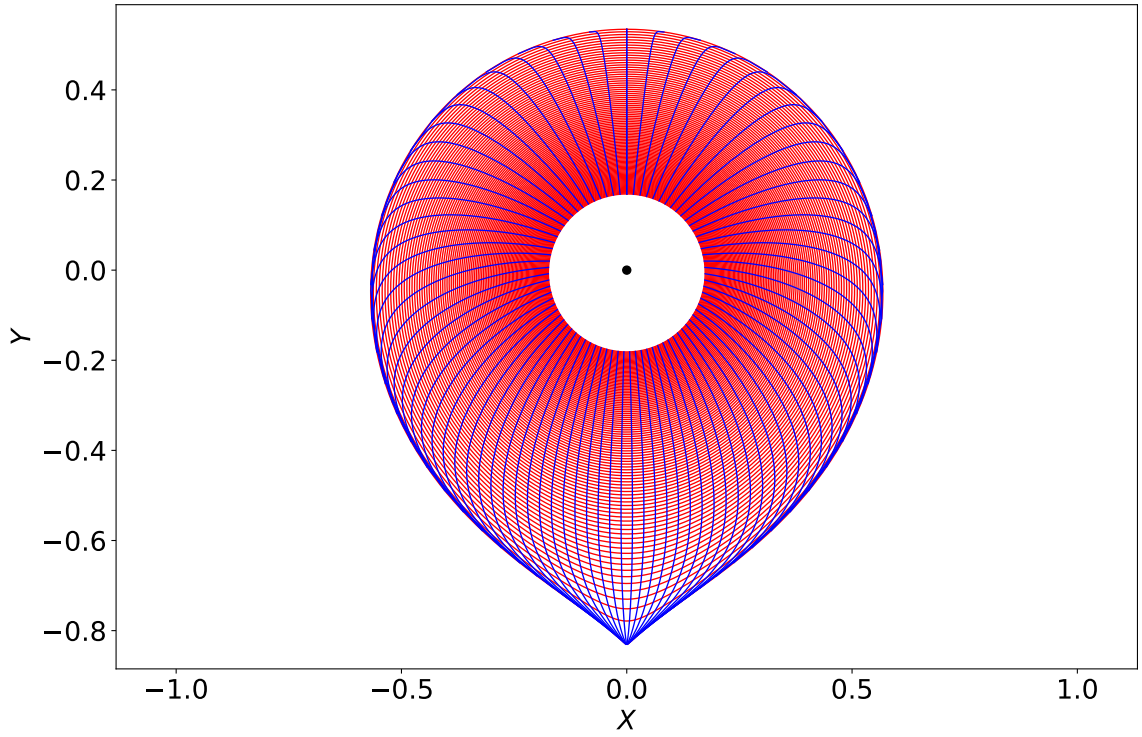

Figure 3. The straight-field-line coordinate system inside the magnetic separatrix. The red curves are surfaces of constant $\hat{\psi}$, whereas the blue curves are surfaces of constant θ. The black dot shows the location of the plasma current filament. Here, $q_* = 12$ and $\zeta = 0.2$.

general, a parallel inductive current is driven on the rational flux-surface. The current is a *shielding current* that acts to suppress driven magnetic reconnection on the flux-surface [5, 19].

We can now appreciate that, by employing a straight-field-line coordinate system, we can distinguish rational magnetic flux-surfaces from irrational flux-surfaces. [A rational surface is one on which the associated safety-factor can be expressed as a rational number. Note that this definition only makes sense if the safety-factor is a flux-surface function. In this respect, we cannot agree with the analysis of Ref. [20] where a coordinate system is adopted in which $q = q(\psi_p, \theta)$ in the vicinity of the X-point.] We can also determine the angular variation of the particular magnetic perturbation that drives a shielding current on a particular rational surface. Finally, it is clear from that Figs. 2–4 that rational flux-surfaces exist both inside and outside the magnetic separatrix.

2.8 Effect of divertor plate

Rational magnetic flux-surfaces exist outside the magnetic separatrix [7] because flux-surfaces in this region form closed loops, that complete below the divertor coil filament, when plotted in the X-Y plane. In fact, this must be the case in an axisymmetric system otherwise the divergence of the magnetic field would be non-zero. Thus, the commonly used term "last closed magnetic flux-surface" (meaning the magnetic separatrix) is inaccurate. All of the magnetic flux-surfaces are closed. However, those outside the magnetic sepatatrix are only partially occupied by plasma because they intersect the solid divertor plate.

Suppose that the divertor plate is horizontal (i.e., parallel to the X-axis), and is situated halfway between the X-point and the divertor coil filament. When integrating Eqs. (14)–(17), we are really integrating along the path of a shielding current filament excited by an inductive electric field. Under normal circumstances, the filament is constrained to run parallel to magnetic field-lines. However, within the rigid divertor plate (which is assumed to be electrically conducting), the filament takes the path of least electrical resistance, which implies that it runs along the X-axis at constant ϕ. It follows that, within the divertor plate, Eqs. (14)–(17) must be replaced by

$$\frac{dX}{dL} = 1, \tag{25}$$

$$\frac{dY}{dL} = 0, \tag{26}$$

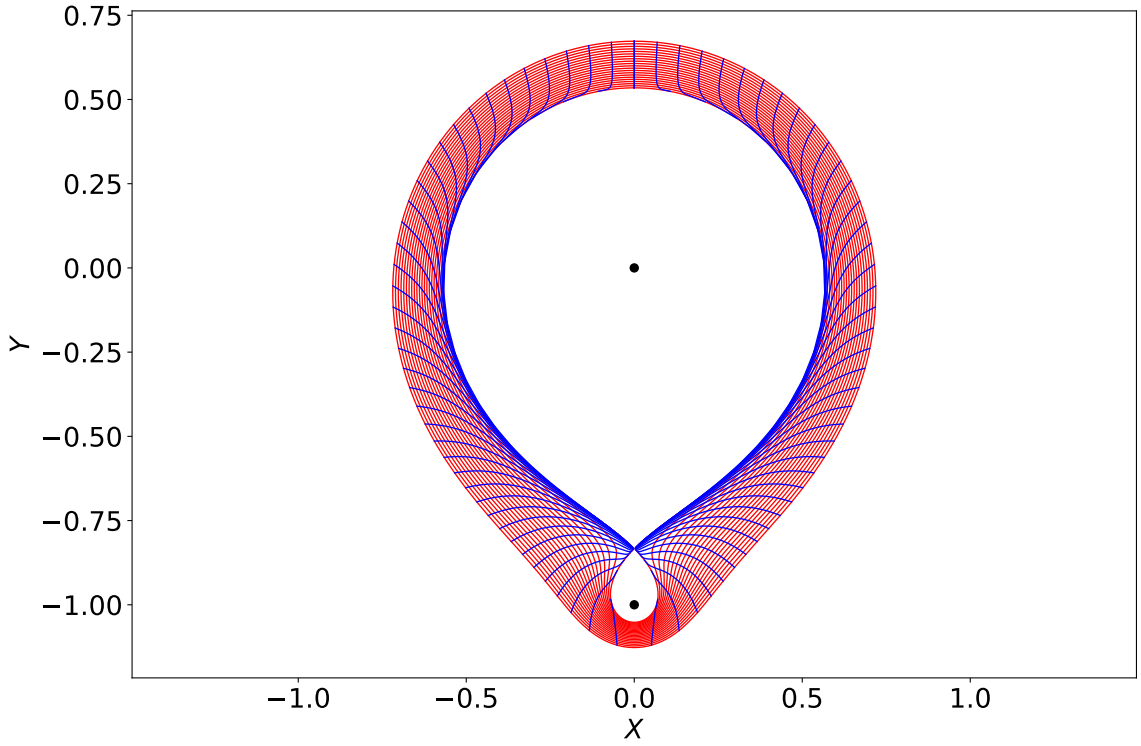

Figure 4. The straight-field-line coordinate system outside the magnetic separatrix in the absence of a divertor plate. The red curves are surfaces of constant $\hat{\psi}$, whereas the blue curves are surfaces of constant θ. The black dots shows the locations of the two current filaments. Here, $q_* = 12$ and $\zeta = 0.2$.

$$\frac{d\phi}{dL} = 0, \tag{27}$$

$$\frac{d\varpi}{dL} = -\frac{Y}{X^2 + Y^2}. \tag{28}$$

Again, let $q_* = 12$ and $\zeta = 0.2$. Figure 5 shows the magnetic flux-surfaces $\Psi = 0.9$, $\Psi = 1.0$, and $\Psi = 1.1$, plotted in the X-Y plane. Note that the surfaces $\Psi = 1.0$ and $\Psi = 1.1$ both have sections that run parallel to the divertor plate. Strictly speaking, these sections are not magnetic flux-surfaces (the actual magnetic flux-surfaces complete below the divertor plate, as shown in Fig. 1), but instead represent the paths of shielding current filaments.

The green curve in Fig. 2 shows the safety-factor profile calculated outside the magnetic separatrix in the presence of the divertor plate. Note that the safety-factor is decreased in the presence of the plate, because shielding current filaments can take a short-cuts through, rather than having to run in loops below, the plate.

Finally, Fig. 6 shows the straight-field-line coordinate system outside the magnetic separatrix in the presence of the divertor plate. Observe that the divertor plate is a surface of constant θ.

3 Improved model of a magnetically diverted plasma

The model described in Sect. 2 has the unrealistic feature that $q = 0$ at the magnetic axis. This feature is an artifact of treating the plasma current as a filament, rather than a spatially extended distribution. In Sect. 3, we shall attempt to construct an improved model.

3.1 Equilibrium magnetic field

Let R, ϕ, Z be conventional cylindrical coordinates that are coaxial with the plasma torus. Thus, $\nabla R \times \nabla\phi \cdot \nabla Z = 1/R$. We can express the equilibrium magnetic field in the divergence-free manner [19]

$$\mathbf{B} = \nabla\phi \times \nabla\psi_p + B_0\, R_0\, g\, \nabla\phi = \nabla(\phi - q\,\theta) \times \nabla\psi_p. \tag{29}$$

Here, ϕ is a true toroidal angle, ψ_p the true poloidal magnetic flux (divided by 2π), $g(\psi_p)$ an arbitrary (dimensionless) flux-function, $q(\psi_p)$ the safety-factor, R_0 the major radius of the magnetic axis, and B_0 the vacuum toroidal magnetic field-strength on the axis (which implies that $g = 1$ in

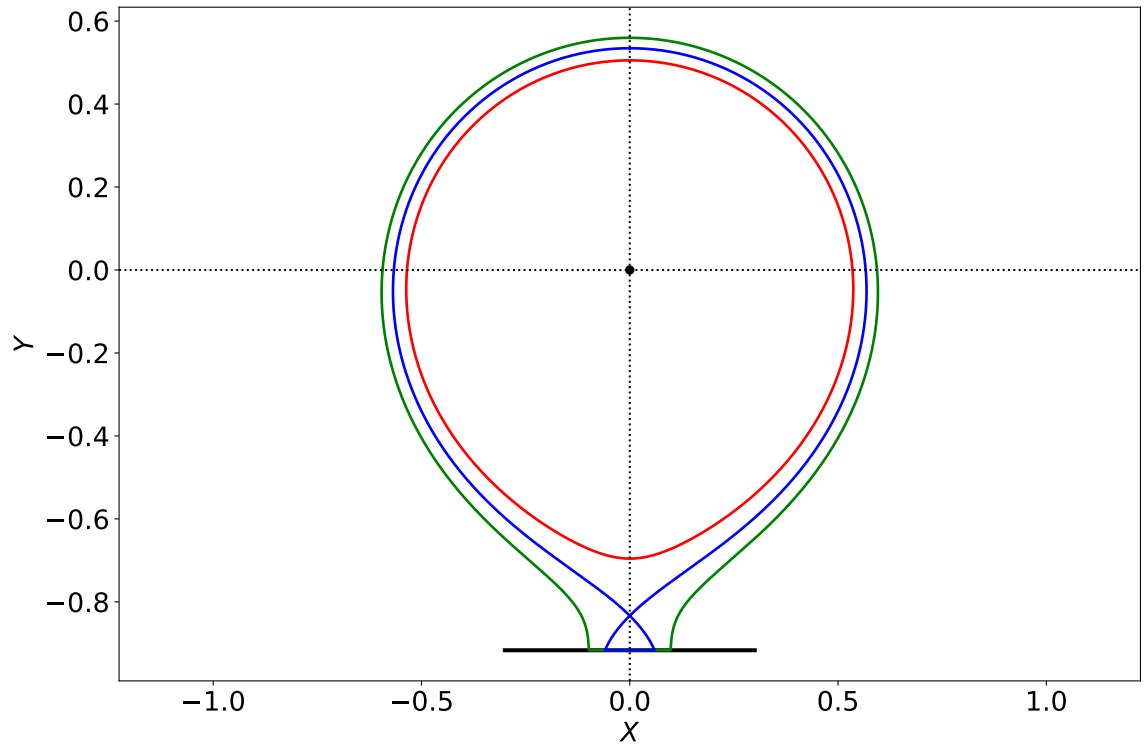

Figure 5. The magnetic flux-surfaces $\Psi = 0.9$ (red), $\Psi = 1.0$ (green), and $\Psi = 1.1$ (blue) in the presence of a divertor plate located halfway between the X-point and the divertor coil filament. The black dot shows the location of plasma current filament, and the horizontal black line shows the location of the divertor plate. Here, $q_* = 12$ amd $\zeta = 0.2$.

the vacuum region surrounding the plasma). The previous equation is only self-consistent if

$$\nabla\psi_p \times \nabla\theta \cdot \nabla\phi = \frac{B_0\, R_0\, g}{R^2\, q}. \tag{30}$$

It is helpful to define a magnetic flux-surface label, r, with the dimensions of length, as follows [19]:

$$\frac{d\psi_p}{dr} = \frac{B_0\, r\, g}{q}. \tag{31}$$

It is easily demonstrated that

$$\nabla r \times \nabla\theta \cdot \nabla\phi = \frac{R_0}{R^2\, r}. \tag{32}$$

Here, r can be interpreted as the mean minor radius of a given magnetic flux-surface. Suppose that the magnetic separatrix corresponds to the flux-surface $r = a$. Thus, we can interpret a as the mean minor radius of the plasma. Moreover, flux-surfaces with $r < a$ lie inside the separatrix, whereas those with $r > a$ lie outside.

3.2 Model safety-factor profile

Let us adopt a model safety-factor profile inspired by the analysis of Sect. 2. Let $\hat{r} = r/a$. Suppose that

$$q(\hat{r}) = q_0 - \alpha_-\, \ln\left(1 - \hat{r}^{\,2}\right) \tag{33}$$

for $\hat{r} < 1$, and

$$q(\hat{r}) = -\alpha_+\, \ln\left(\hat{r}^{\,2} - 1\right) \tag{34}$$

for $\hat{r} > 1$, where

$$\alpha_- = -\frac{q_{95} - q_0}{\ln(1 - \hat{r}_{95}^2)}, \tag{35}$$

$$\alpha_+ = -\frac{q_{105}}{\ln(\hat{r}_{105}^2 - 1)}. \tag{36}$$

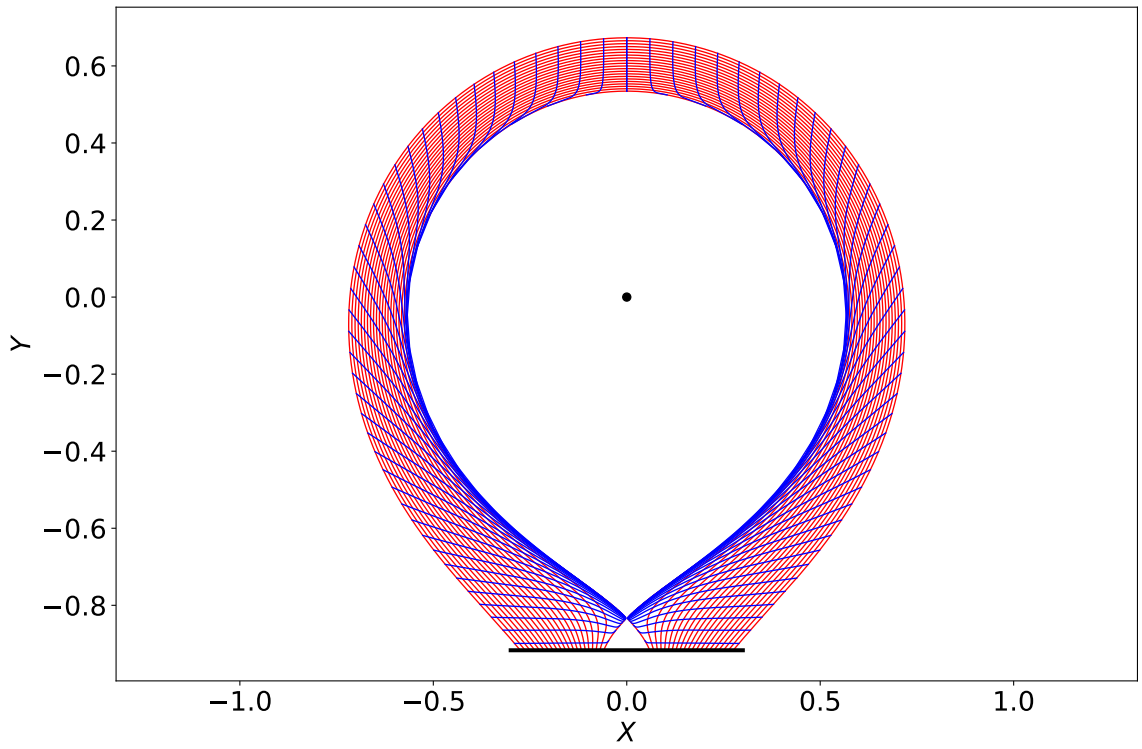

Figure 6. The straight-field-line coordinate system outside the magnetic separatrix in the presence of a divertor plate located halfway between the X-point and the divertor coil filament. The red curves are surfaces of constant $\hat{\psi}$, whereas the blue curves are surfaces of constant θ. The black dot shows the location of the plasma current filament, and the horizontal black line shows the location of the divertor plate. Here, $q_* = 12$ and $\zeta = 0.2$.

Here, q_0 is the safety-factor on the magnetic axis ($\hat{r} = 0$), q_{95} is the safety-factor on the magnetic flux-surface that encloses 95% of the poloidal magnetic flux enclosed by the magnetic separatrix, $\hat{r}_{95}$ is the $\hat{r}$-coordinate of the 95% flux-surface, q_{105} is the safety-factor on the magnetic flux-surface that encloses 105% of the poloidal magnetic flux enclosed by the magnetic separatrix, and $\hat{r}_{105}$ is the $\hat{r}$-coordinate of the 105% flux-surface.

3.3 Poloidal magnetic flux

We wish to determine the poloidal flux in the vicinity of the magnetic separatrix. Let $\psi_p = B_0\, a^2\, \psi$. It follows from Eq. (31) that

$$\frac{d\psi}{d\hat{r}} \simeq \frac{\hat{r}}{q}, \tag{37}$$

assuming that we can set $g \simeq 1$ close to the separatrix.

For $\hat{r} < 1$, Eqs. (33) and (37) yield

$$\frac{d\psi}{d\hat{r}} = \frac{\hat{r}}{q_0 - \alpha_-\, \ln(1-\hat{r}^{\,2})}, \tag{38}$$

which can be integrated to give

$$\psi(\hat{r}) = \frac{\mathrm{e}^{\,q_0/\alpha_-}}{2\,\alpha_-}\left\{E_1\left(\frac{q_0}{\alpha_-}\right) - E_1\left[\frac{q_0}{\alpha_-} - \ln\left(1-\hat{r}^{\,2}\right)\right]\right\}, \tag{39}$$

where $E_1(x)$ is an exponential integral [21]. Hence,

$$\psi(1) = \frac{\mathrm{e}^{\,q_0/\alpha_-}}{2\,\alpha_-}\, E_1\left(\frac{q_0}{\alpha_-}\right) \tag{40}$$

is the poloidal magnetic flux (divided by $2\pi\, B_0\, a^2$) enclosed within the magnetic separatrix. Let us define the *normalized poloidal magnetic flux*, $\Psi(\hat{r}) = \psi(\hat{r})/\psi(1)$. Thus, $\Psi = 0$ on the magnetic axis, $\Psi = 1$ on the magnetic separatrix, and $\Psi > 1$ outside the separatrix. It follows that

$$\Psi(\hat{r}) = 1 - \frac{E_1[q_0/\alpha_- - \ln(1-\hat{r}^{\,2})]}{E_1(q_0/\alpha_-)} = 1 - \frac{E_1(q/\alpha_-)}{E_1(q_0/\alpha_-)}. \tag{41}$$

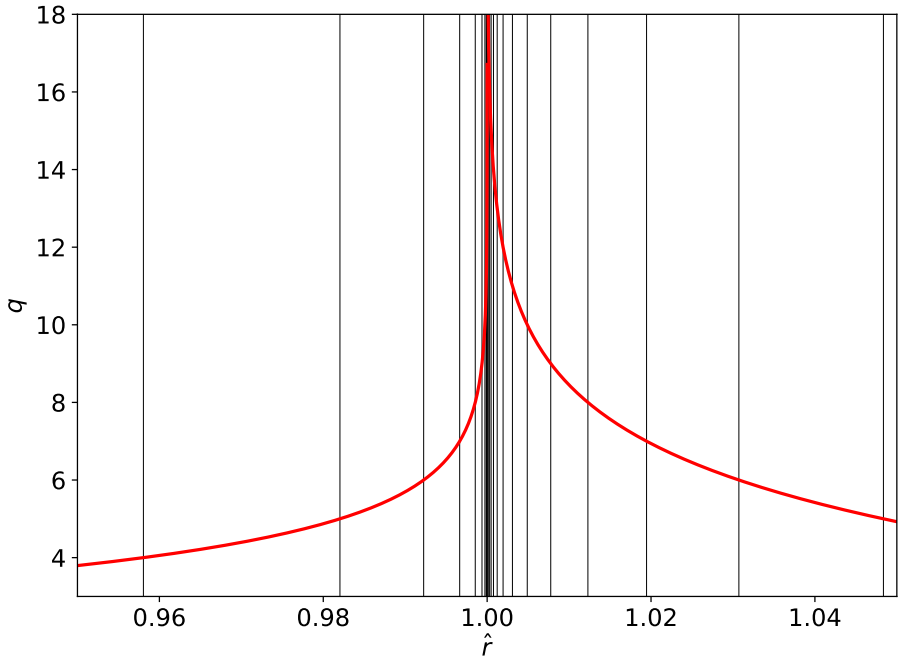

Figure 7. The model safety-factor profile in the vicinity of the magnetic separatrix, calculated for $q_0 = 1.01$, $q_{95} = 3.5$, and $q_{105} = 4.0$. The black vertical lines show the locations of the $n = 1$ rational surfaces.

By definition, $\Psi(\hat{r}_{95}) = 0.95$, so

$$\frac{E_1(q_{95}/\alpha_-)}{E_1(q_0/\alpha_-)} = 0.05. \tag{42}$$

Assuming that q_0 and q_{95} are specified, the previous equation can be solved to give α_-, which then allows $\hat{r}_{95}$ to be determined from Eq. (35).

For $\hat{r} > 1$, Eqs. (34) and (37) yield

$$\frac{d\psi}{d\hat{r}} = -\frac{\hat{r}}{\alpha_+ \ln(\hat{r}^{\,2} - 1)}, \tag{43}$$

which can be integrated to give

$$\psi(\hat{r}) = \psi(1) + \frac{E_1[-\ln(\hat{r}^{\,2} - 1)]}{2\,\alpha_+}. \tag{44}$$

Thus,

$$\Psi(\hat{r}) = 1 + \frac{\alpha_-}{\alpha_+}\,\mathrm{e}^{-q_0/\alpha_-}\,\frac{E_1[-\ln(\hat{r}^{\,2} - 1)]}{E_1(q_0/\alpha_-)} = 1 + \frac{\alpha_-}{\alpha_+}\,\mathrm{e}^{-q_0/\alpha_-}\,\frac{E_1(q/\alpha_+)}{E_1(q_0/\alpha_-)}, \tag{45}$$

where use has been made of Eq. (40). By definition, $\Psi(\hat{r}_{105}) = 1.05$. Hence, Eqs. (42) and (45) can be combined to give

$$\frac{E_1(q_{105}/\alpha_+)}{\alpha_+} = \mathrm{e}^{\,q_0/\alpha_-}\,\frac{E_1(q_{95}/\alpha_-)}{\alpha_-}. \tag{46}$$

Assuming that q_{105} is specified, the previous equation can be solved to give α_+, which then allows $\hat{r}_{105}$ to be determined from Eq. (36).

Consider a plasma equilibrium characterized by $q_0 = 1.01$, $q_{95} = 3.5$, and $q_{105} = 4.0$. We can solve Eqs. (42) and (46) to give $\alpha_- = 1.196$ and $\alpha_+ = 2.163$. Equations (35) and (36) then reveal that $\hat{r}_{95} = 0.9355$ and $\hat{r}_{105} = 1.076$. The resulting model safety-factor profile in the vicinity of the magnetic separatrix is shown in Fig. 7.

4 Plasma response theory

The aim of Sect. 4 is to analyze the response of a tokamak plasma possessing a magnetic separatrix to a static RMP of toroidal mode number n.

4.1 Ideal-MHD perturbation

Suppose that the plasma equilibrium is subject to a static magnetic perturbation that possesses n periods in the toroidal direction, and is such that [22]

$$\frac{r\,b^r(r,\theta,\phi)}{B_0\,R_0} = \mathrm{i}\left(\frac{R_0}{R}\right)^2 \sum_m \psi_m(r)\,\mathrm{e}^{\,\mathrm{i}\,(m\,\theta - n\,\phi)}, \tag{47}$$

where $b^r = \mathbf{b}\cdot\nabla r$, $\mathbf{b}$ is the perturbed magnetic field, and the $\psi_m(r)$ are dimensionless functions. Note that the perturbation consists of a single toroidal harmonic, but multiple poloidal harmonics, characterized by the set of integer poloidal mode numbers m. As is well known, this is the case because, whereas different toroidal harmonics are not coupled together in an axisymmetric plasma equilibrium, different poloidal harmonics are coupled by the Shafranov shift and shaping of the equilibrium magnetic flux-surfaces [19]. Everywhere in the plasma, apart from the immediate vicinity of the various rational surfaces, the perturbation is governed by the linearized equations of inertia-free (because the perturbation is static, and the plasma equilibrium remains an equilibrium in the presence of the perturbation) ideal-magnetohydrodynamics (MHD) [24]. These equations reduce to a set of coupled ordinary differential equations (o.d.e.s) that take the form [19, 22]

$$r\,\frac{d\psi_m}{dr} = \sum_{m'} \frac{L_m^{m'}\,Z_{m'} + M_m^{m'}\,\psi_{m'}}{m' - n\,q}, \tag{48}$$

$$(m - n\,q)\,r\,\frac{d}{dr}\left(\frac{Z_m}{m - n\,q}\right) = \sum_{m'} \frac{N_m^{m'}\,Z_{m'} + P_m^{m'}\,\psi_{m'}}{m' - n\,q}. \tag{49}$$

Here, the (dimensionless) $Z_m(r)$ functions are related to the poloidal harmonics of the perturbed toroidal magnetic field. Moreover, the (dimensionless) $L_m^{m'}(r)$, $M_m^{m'}(r)$, $N_m^{m'}(r)$, and $P_m^{m'}(r)$ coefficients are determined by the equilibrium profiles and the metric elements of the r, θ, ϕ straight-field-line coordinate system [22]. In particular, $L_m^m(r)$ controls the radial wavelength of the m, n tearing mode, $P_m^m(r)$ encodes the destabilizing effect of equilibrium current and pressure gradients on the mode, whereas the $N_m^{m'}(r)$ the $M_m^{m'}(r)$ and the off-diagonal elements of the $L_m^{m'}(r)$ and the $P_m^{m'}(r)$ control the coupling between tearing modes with different poloidal mode numbers in a toroidal plasma equilibrium with a shaped poloidal cross-section. Note that Eqs. (48) and (49) are singular at rational magnetic flux-surfaces at which $q = m/n$.

The locations of the $n = 1$ rational surfaces for our model safety-factor profile are indicated in Fig. 7. It can be seen that rational surfaces accumulate in the vicinity of the magnetic separatrix, where $q(\hat{r})$ has a logarithmic singularity. Moreover, rational surfaces exist both inside and outside the separatrix.

4.2 Behavior in vicinity of rational surface

Consider the solution of the ideal-MHD o.d.e.s, (48) and (49), in the vicinity of a rational surface, of radius r_s, where $q(r_s) = m/n$, and m is the resonant poloidal mode number. Let $x = r - r_s$. At small values of $|x|$, the function $\psi_m(r)$ takes the form [19, 22]

$$\psi_m(r_s + x) = A_L^{\pm}\,|x|^{\,\nu_L}(1 + \lambda_L\,x) + A_S^{\pm}\,\mathrm{sgn}(x)\,|x|^{\,\nu_S} + A_C\,x + \mathcal{O}(x^2), \tag{50}$$

where

$$\nu_L = \frac{1}{2} - \sqrt{-D_I}, \tag{51}$$

$$\nu_S = \frac{1}{2} + \sqrt{-D_I}, \tag{52}$$

$$D_I = -L_0\,P_0 - \frac{1}{4}, \tag{53}$$

$$L_0 = -\left(\frac{L_m^m}{m\,s}\right)_{r_s}, \tag{54}$$

$$P_0 = -\left(\frac{P_m^m}{m\,s}\right)_{r_s}, \tag{55}$$

$$s = \frac{d\ln q}{d\ln r}, \tag{56}$$

and λ_L and A_C are defined in Refs. [19] and [22]. The superscripts + and − correspond to $x > 0$ and $x < 0$, respectively. Here, $A_L^{\pm}$ are known as the *coefficients of the large solution*, whereas $A_S^{\pm}$ are termed the *coefficients of the small solution*. The *Mercier interchange stability parameter*, D_I, is assumed to be negative. (Otherwise, the plasma in the vicinity of the rational surface would be unstable to localized ideal interchange modes [25].) Note that ν_L and ν_S are known as *Mercier indices*. Moreover, s is the magnetic shear,

In general, the response of the plasma in the vicinity of a given rational surface to the RMP is predominately *tearing parity* in nature [23]. For the case of a tearing parity response, the coefficients of the large solution to the left and the right of a rational surface are equal to one another. In other words, $A_L^+ = A_L^- = A_L$. Note, however, that the coefficients of the small solution to the left and the right of a rational surface are not, in general, equal to one another.

4.3 Plasma response equation

Let us index the various rational surfaces in the plasma by means of an integer k. Note that this is possible even if there are an infinite number of such surfaces. Thus, the kth rational surface possesses the minor radius r_k, the resonant poloidal mode number m_k, the coefficient of the large solution $A_{L\,k}$, the coefficients of the small solution $A_{S\,k}^{\pm}$, and the Mercier indices $\nu_{L\,k}$ and $\nu_{S\,k}$. It is helpful to define the quantities [19, 22]

$$\Psi_k = r_k^{\nu_{L\,k}} \left(\frac{\nu_{S\,k} - \nu_{L\,k}}{L_{m_k}^{m_k}} \right)_{r_k}^{1/2} A_{L\,k}, \tag{57}$$

$$\Delta\Psi_k = r_k^{\nu_{S\,k}} \left(\frac{\nu_{S\,k} - \nu_{L\,k}}{L_{m_k}^{m_k}} \right)_{r_k}^{1/2} (A_{S\,k}^+ - A_{S\,k}^-). \tag{58}$$

at each rational surface. Here, the complex dimensionless parameter Ψ_k is a measure of the driven reconnected magnetic flux at the kth rational surface, whereas the complex dimensionless parameter $\Delta\Psi_k$ is a measure of the strength of the radially localized shielding current that flows around the surface.

The response of a tokamak plasma to an RMP takes the general form [19, 22]

$$\Delta\Psi_k = \sum_{k'} E_{kk'}\,\Psi_{k'} + \chi_k, \tag{59}$$

and specifies the shielding current that is excited in the vicinity of the kth rational surface in response to reconnected magnetic flux at the other rational surfaces, as well as to the RMP. Here, $E_{kk'}$ is an Hermitian matrix that can be determined entirely from the ideal-MHD o.d.e.s, (48) and (49), subject to physical boundary conditions at small and large r [19, 22]. Moreover, the real quantity E_{kk} can be interpreted as the *tearing stability index* [24] of a tearing mode that only reconnects magnetic flux at the kth rational surface. The off-diagonal elements of $E_{kk'}$ specify the coupling between tearing modes that reconnect magnetic flux at different rational surfaces. Finally, the χ_k specify the poloidal harmonics of the RMP [22, 23].

4.4 Resistive layers

In reality, the shielding current that flows in the vicinity of the kth rational surface does so in a resistive layer whose thickness (in r), δ_k, is much less than r_k [24]. We can define the complex dimensionless *layer response index*,

$$\Delta_k \equiv \frac{\Delta\Psi_k}{\Psi_k}, \tag{60}$$

which characterizes the tearing parity response of the plasma in the layer to the magnetic perturbation external to the layer. Equations (59) and (60) can be combined to give

$$\sum_{k'} (\Delta_k\,\delta_{kk'} - E_{kk'})\,\Psi_k = \chi_k, \tag{61}$$

where $\delta_{kk'}$ is a Kronecker delta symbol. The previous equation is termed the *plasma response equation*, and specifies the reconnected magnetic flux driven by the RMP at each rational surface in the plasma.

Note that the derivation of Eq. (61) depends crucially on the principle of *asymptotic matching* [24]. According to this principle, the plasma response is governed by the equations of linearized, marginally-stable, ideal-MHD throughout most of the plasma. However, these equations become

singular at the various rational surfaces in the plasma. [See Eqs. (48) and (49).] The singularities are resolved by asymptotically matching the ideal-MHD solution to resistive layer solutions at each rational surface in the plasma.

4.5 Ideal and vacuum responses

Suppose, for the sake of argument, that the plasma only contains a single rational surface. In this case, the plasma response equation, (61), reduces to

$$\Psi_k = \frac{\chi_k}{\Delta_k - E_{kk}}. \tag{62}$$

Alternatively, Eq. (59) yields

$$\Delta\Psi_k = E_{kk}\,\Psi_k + \chi_k. \tag{63}$$

Let us suppose that $E_{kk} < 0$: i.e., the tearing mode resonant at the surface is intrinsically stable. In this case, any magnetic reconnection that takes place at the surface is entirely due to the RMP. We can distinguish two asymptotic limits. In the first limit, $|\Delta_k| \gg (-E_{kk})$. In this limit, the shielding current excited at the rational surface is sufficiently strong that driven magnetic reconnection is largely suppressed at the surface [5, 19]. In other words, $\Psi_k \simeq 0$. We term this an *ideal response*, because it is the exactly the same response as one would get by imposing the ideal-MHD flux-freezing constraint that the topology of the magnetic field cannot change at the rational surface: i.e., $\Psi_k = 0$ [3]. In the second limit, $|\Delta_k| \ll (-E_{kk})$. In this limit, the shielding current is too weak to prevent driven magnetic reconnection from occurring at the rational surface. Thus, $\Psi_k \simeq \chi_k/(-E_{kk})$. We term this a *vacuum response*, because it is exactly the same response as one would get by imposing the vacuum constraint that no shielding current flows at the rational surface: i.e., $\Delta\Psi_k = 0$.

In a region of the plasma in which the response to the RMP lies in the ideal regime [i.e., $|\Delta_k|/(-E_{kk}) \gg 1$ at all rational surfaces], the perturbed magnetic field has a strong dependence on the equilibrium magnetic field, because the equilibrium field determines the locations of the rational surfaces on which the constraints $\Psi_k = 0$ have to be imposed. On the other hand, in a region of the plasma in which the response lies in the vacuum regime [i.e., $|\Delta_k|/(-E_{kk}) \ll 1$ at all rational surfaces], the perturbed magnetic field has no (local) dependence on the equilibrium magnetic field. This is the case because we can write the perturbed field in a current-free region in the form $\mathbf{b} = \nabla V$, where the vacuum potential satisfies $\nabla^2 V = 0$, which completely independent of the equilibrium field. Moreover, writing the perturbed magnetic field in this form automatically satisfies the constraints that $\Delta\Psi_k = 0$ at the rational surfaces. Thus, in the vacuum regime, there is no need for us to determine the locations of the rational surfaces, which means that we do not have to employ a straight-field-line coordinate system, which implies that there is no reason for our adopted coordinate system to become singular anywhere.

In reality, the plasma contains many rational surfaces. In this case, Eq. (62) generalizes to give

$$\boldsymbol{\Psi} = (\boldsymbol{\Delta} - \mathbf{E})^{-1}\,\boldsymbol{\chi}, \tag{64}$$

where $\boldsymbol{\Psi}$ is the vector of the Ψ_k values, $\boldsymbol{\Delta}$ the diagonal matrix of the Δ_k values, $\mathbf{E}$ the matrix of the $E_{kk'}$ values, and $\boldsymbol{\chi}$ the vector of the χ_k values. For the case of two rational surfaces, we get

$$\Psi_1 = \frac{(\Delta_2 - E_{22})\,\chi_1 + E_{12}\,\chi_2}{(\Delta_1 - E_{11})\,(\Delta_2 - E_{22}) - E_{12}\,E_{21}}, \tag{65}$$

$$\Psi_2 = \frac{E_{21}\,\chi_1 + (\Delta_1 - E_{11})\,\chi_2}{(\Delta_1 - E_{11})\,(\Delta_2 - E_{22}) - E_{12}\,E_{21}}. \tag{66}$$

Now, we expect rational surfaces close to the magnetic separatrix to have large associated poloidal mode numbers. In the cylindrical limit, $E_{kk} = -2\,m_k$. In toroidal geometry, E_{kk} differs somewhat from $-2\,m_k$. However, as can be demonstrated from toroidal tearing mode codes such as TJ [22], it is still the case that E_{kk} is large and negative, and $E_{kk} \propto -m_k$. In other words, it remains true that $E_{kk} \sim -2\,m_k$. Moreover, the magnitudes of the off-diagonal elements of the E-matrix also scale as m_k. Finally, we expect neighboring rational surfaces to have similar Δ_k values. Thus, if $|\Delta_1|, |\Delta_2| \gg |E_{11}|, |E_{22}|, |E_{12}|, |E_{21}| \sim 2\,m_1$ then Eqs. (65) and (66) yield

$$\Psi_1 \simeq \frac{\chi_1}{\Delta_1}, \tag{67}$$

$$\Psi_2 \simeq \frac{\chi_2}{\Delta_2}. \tag{68}$$

On the other hand, if $|\Delta_1|$, $|\Delta_2| \ll |E_{11}|$, $|E_{22}|$, $|E_{12}|$, $|E_{21}| \sim 2\,m_1$ then we get

$$\Psi_1 \simeq \frac{-E_{22}\,\chi_1 + E_{12}\,\chi_2}{E_{11}\,E_{12} - E_{12}\,E_{21}}, \tag{69}$$

$$\Psi_2 \simeq \frac{E_{21}\,\chi_1 - E_{11}\,\chi_2}{E_{11}\,E_{12} - E_{12}\,E_{21}}. \tag{70}$$

Equations (69) and (70) correspond to a vacuum response, in which the reconnected flux driven at the rational surfaces is the same as that which would occur in a vacuum. On the other hand, Eqs. (67) and (68) correspond to an ideal response, in which the reconnected flux driven at the rational surfaces is strongly suppressed by shielding currents. It is clear that the criterion for the latter response is $|\Delta_1| \gg 2\,m_1 \sim (-E_{11})$, whereas that for the former response is $|\Delta_1| \ll 2\,m_1 \sim (-E_{11})$. We can generalize the previous analysis to the case of many rational surfaces close to the magnetic separatrix. The conclusion remains that a ideal response corresponds to $|\Delta_k| \gg (-E_{kk})$, whereas a vacuum response corresponds to $|\Delta_k| \ll (-E_{kk})$.

5 Behavior close to magnetic separatrix

The aim of Sect. 5 is to investigate asymptotic matching in the immediate vicinity of the magnetic separatrix.

5.1 Spacing between successive rational surfaces

Suppose that $\hat{r}_{k+1} > \hat{r}_k$ for all values of k, where $\hat{r}_k = r_k/a$. In other words, suppose that the rational surfaces are indexed in order of increasing minor radius. In the vicinity of the magnetic separatrix, Eqs. (33) and (34) yield

$$\hat{r}_k \simeq \left[1 - \exp\left(-\frac{m_k}{n\,\alpha_-}\right)\right]^{1/2} \tag{71}$$

for $\hat{r}_k < 1$, and

$$\hat{r}_k = \left[1 + \exp\left(-\frac{m_k}{n\,\alpha_+}\right)\right]^{1/2} \tag{72}$$

for $\hat{r}_k > 1$.

The spacing (in $\hat{r}$) between successive rational surfaces is

$$\hat{\epsilon}_k(\hat{r}_k) = \frac{d\hat{r}_k}{dm_k} \tag{73}$$

for $\hat{r}_k < 1$, and

$$\hat{\epsilon}_k(\hat{r}_k) = -\frac{d\hat{r}_k}{dm_k} \tag{74}$$

for $\hat{r}_k > 1$. Thus,

$$\hat{\epsilon}_k(\hat{r}_k) = \frac{1 - \hat{r}_k^2}{2\,n\,\alpha_-\,\hat{r}_k} \tag{75}$$

for $\hat{r}_k < 1$, and

$$\hat{\epsilon}_k(\hat{r}_k) = \frac{\hat{r}_k^2 - 1}{2\,n\,\alpha_+\,\hat{r}_k} \tag{76}$$

for $\hat{r}_k > 1$. Note that the spacing between successive rational surfaces tends to zero linearly as the magnetic separatrix ($\hat{r}_k = 1$) is approached.

5.2 Magnetic shear

In the vicinity of the magnetic separatrix, the magnetic shear can be written

$$s(\hat{r}) \equiv \frac{\hat{r}}{q}\,\frac{dq}{d\hat{r}} \simeq -\frac{1}{(\hat{r}-1)\,\ln(2\,|\hat{r}-1|)}. \tag{77}$$

Observe that the magnitude of the shear becomes infinite as the magnetic separatrix ($\hat{r} = 1$) is approached.

5.3 Resistive layer quantities

It is helpful to define the following quantities that parameterize a general resistive layer [26]:

$$\ln\Lambda = 24 - \ln\left[\left(\frac{n_e}{10^6}\right)^{1/2}\left(\frac{e}{T_e}\right)\right], \tag{78}$$

$$\tau_{ei} = \frac{6\sqrt{2}\,\pi^{3/2}\,\epsilon_0^2\,m_e^{1/2}\,T_e^{3/2}}{Z\,\ln\Lambda\,e^4\,n_e}, \tag{79}$$

$$\eta_\parallel = \frac{m_e}{1.96\,n_e\,e^2\,\tau_{ei}}, \tag{80}$$

$$\tau_R = \frac{\mu_0\,r^2}{\eta_\parallel}, \tag{81}$$

$$\tau_A = \frac{R_0\,\sqrt{\mu_0\,m_i\,n_e}}{B_0}, \tag{82}$$

$$\tau_E = \frac{r^2}{\chi_E}, \tag{83}$$

$$\tau_\phi = \frac{r^2}{\chi_\phi}, \tag{84}$$

$$d_\beta = \frac{\sqrt{(5/3)\,m_i\,(T_e+T_i)}}{e\,B_0}, \tag{85}$$

$$S = \frac{\tau_R}{\tau_A}. \tag{86}$$

Here, Z is the effective ion charge number, $T_e(r)$ the electron temperature, $T_i(r)$ the ion temperature, m_e the electron mass, m_i the ion mass, $\chi_E(r)$ the perpendicular energy diffusivity, and $\chi_\phi(r)$ the perpendicular momentum diffusivity. Furthermore, $\tau_R(r)$ is the resistive diffusion time, $\tau_A(r)$ the Alfvén time, $\tau_E(r)$ the energy confinement time, $\tau_\phi(r)$ the momentum confinement time, $d_\beta(r)$ the ion sound-radius, and $S(r)$ the Lundquist number.

5.4 Resistive layer equation

Let $Y(r)\,\exp[\mathrm{i}\,(m\,\theta - n\,\phi)]$ represent the perturbed electron fluid stream-function in the laboratory frame. Consider the resistive layer centered on the kth rational surface. Let $X = S^{\,1/3}\,(r-r_k)/r_k$, where S is evaluated at radius r_k. We can write

$$\overline{Y}(p) = \int_{-\infty}^{\infty} Y(X)\,\mathrm{e}^{-\mathrm{i}\,p\,X}\,dX. \tag{87}$$

The boundary conditions are that $\overline{Y}(p)\rightarrow 0$ as $p\rightarrow\infty$, and

$$\overline{Y}(p) = Y_0\left[\frac{S^{-1/3}\,\Delta_k}{\pi\,p} + 1 + \mathcal{O}(p)\right] \tag{88}$$

at small values of p [26, 27]. Here, Y_0 is an arbitrary constant, and Δ_k is the complex (dimensionless) layer response index introduced in Eq. (60).

Suppose that the resistive layer physics is controlled by the low-β, three-field, extended-MHD model described in Ref. [26]. In this case, the Fourier transformed layer equations reduce to the following equation:

$$\frac{d}{dp}\left[A(p)\,\frac{d\overline{Y}}{dp}\right] - \frac{B(p)}{C(p)}\,p^2\,\overline{Y} = 0, \tag{89}$$

where

$$A(p) = \frac{(n\,s)^2\,p^2}{\mathrm{i}\,(Q_E+Q_e)+p^2}, \tag{90}$$

$$B(p) = -Q_E\,(Q_E+Q_i) + \mathrm{i}\,(Q_E+Q_i)\,(P_\phi+P_E)\,p^2 + P_\phi\,P_E\,p^4, \tag{91}$$

$$C(p) = \mathrm{i}\,(Q_E+Q_e) + \left[P_E + \mathrm{i}\,(Q_E+Q_i)\,D^{\,2}\right]p^2 + (1+1/\tau)\,P_\phi\,D^{\,2}\,p^4. \tag{92}$$

Here,

$$\tau = -\frac{\omega_{*\,e}}{\omega_{*\,i}}, \tag{93}$$

$$Q_E = -S^{1/3}\, n\, \omega_E\, \tau_A, \tag{94}$$

$$Q_{e,i} = -S^{1/3}\, n\, \omega_{*\,e,i}\, \tau_A, \tag{95}$$

$$D = S^{1/3} \left(\frac{\tau}{1+\tau}\right)^{1/2} \hat{d}_\beta, \tag{96}$$

$$P_E = \frac{\tau_R}{\tau_E}, \tag{97}$$

$$P_\phi = \frac{\tau_R}{\tau_\phi}, \tag{98}$$

and

$$\omega_{*\,i}(r) = -\frac{1}{e\, n_e}\, \frac{dp_i}{d\psi_p} \tag{99}$$

is the *ion diamagnetic frequency*. Moreover, $p_i(r)$ is the equilibrium ion pressure, and $\hat{d}_\beta = d_\beta/r$. As before, all quantities are evaluated at radius r_k. Note that Q_E is the normalized $\mathbf{E}\times\mathbf{B}$ frequency, Q_e the normalized electron diamagnetic frequency, Q_i the normalized ion diamagnetic frequency, D the normalized ion sound-radius, P_E the magnetic Prandtl number associated with anomalous cross-flux-surface energy diffusion, and P_ϕ the magnetic Prandtl number associated with anomalous cross-flux-surface ion momentum diffusion.

5.5 Solution of resistive layer equation

As we saw in Sect. 5.2, the magnetic shear becomes very large as the magnetic separatrix is approached. If we treat $(n\,s)^2$ as much larger than the other parameters (e.g., Q_E, Q_e, P_E, D) that appear in Eqs. (89)–(92) (see Fig. 9) then it is clear that the first term on the left-hand side of Eq. (89) dominates the second term in the region $p \lesssim 1$. In this case, we can integrate the equation to give

$$\overline{Y}(p) = Y_0 \left\{ \frac{S^{-1/3}\,\Delta_k}{\pi} \left[\frac{1}{p} + \frac{p}{-\mathrm{i}\,(Q_E+Q_e)}\right] + 1 + \mathcal{O}(p^2)\right\} \tag{100}$$

for $p \lesssim 1$, where use has been made of Eq. (88). Incidentally, the previous equation bears the hallmark of a *constant-ψ* layer response regime [24, 26].

Let $p = (n\,|s|)^{1/2}\,\hat{p}$. For $\hat{p} \gtrsim 1$, Eqs. (89)–(92) yield

$$\frac{d^2\overline{Y}}{d\hat{p}^{\,2}} - \frac{B(\hat{p})}{C(\hat{p})}\,\hat{p}^{\,2}\,\overline{Y} \simeq 0, \tag{101}$$

where

$$\begin{aligned} B(\hat{p}) &= -Q_E\,(Q_E+Q_i) + \mathrm{i}\,(Q_E+Q_i)\,(P_\phi+P_E)\,(n\,|s|)\,\hat{p}^{\,2} + P_\phi\,P_E\,(n\,|s|)^2\,\hat{p}^{\,4} \\ &\simeq P_\phi\,P_E\,(n\,|s|)^2\,\hat{p}^{\,4}, \end{aligned} \tag{102}$$

$$\begin{aligned} C(\hat{p}) &= \mathrm{i}\,(Q_E+Q_e) + \left[P_E + \mathrm{i}\,(Q_E+Q_i)\,D^{\,2}\right](n\,|s|)\,\hat{p}^{\,2} + (1+1/\tau)\,P_\phi\,D^{\,2}\,(n\,|s|)^2\,\hat{p}^{\,4} \\ &\simeq (1+1/\tau)\,P_\phi\,D^{\,2}\,(n\,|s|)^2\,\hat{p}^{\,4}, \end{aligned} \tag{103}$$

which reduces to

$$\frac{d^2\overline{Y}}{dp^2} - G\,p^2\,\overline{Y} \simeq 0, \tag{104}$$

where

$$G = \frac{P_E}{(1+1/\tau)\,D^{\,2}\,n^2\,|s|^2} = \frac{\tau_A^{\,2/3}\,\tau_R^{\,1/3}}{\tau_E\,\hat{d}_\beta^{\,2}\,(n\,|s|)^2}. \tag{105}$$

In the language of Ref. [26], we have found a constant-ψ layer solution characterized by $\nu = 1/4$. It follows from the analysis of Ref. [26] that

$$S^{-1/3}\,\Delta_k = \frac{\nu^{\,2\nu-1}\pi\,\Gamma(1-\nu)}{\Gamma(\nu)}\,[\mathrm{i}\,(Q_E+Q_e)]\,G^{\,\nu}, \tag{106}$$

where $\Gamma(z)$ is a gamma function [21]. Hence, in the continuum limit in which the resistive layers are very closely spaced,

$$\Delta_k(\hat{r}) = -\mathrm{i}\,\frac{2\pi\,\Gamma(3/4)}{\Gamma(1/4)}\,\frac{n\,(\omega_E+\omega_{*\,e})\,\tau_A^{\,1/2}\,\tau_R^{\,3/4}}{\tau_E^{\,1/4}\,\hat{d}_\beta^{\,1/2}\,(n\,|s|)^{1/2}}, \tag{107}$$

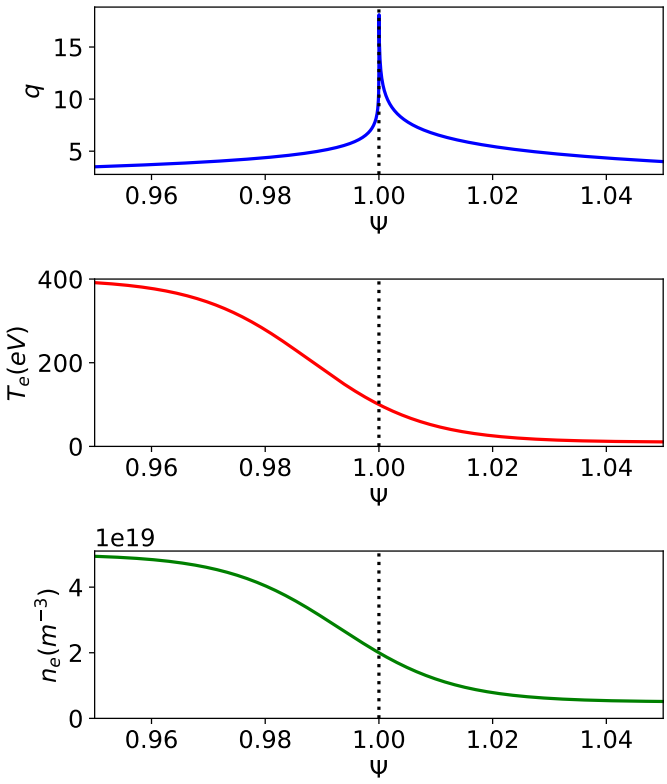

Figure 8. Model safety-factor, electron temperature, and electron number density profiles at the edge of a typical JET H-mode plasma. The vertical dotted lines show the location of the magnetic separatrix.

where all terms on the right-hand side are evaluated at the normalized radius $\hat{r}$. Thus, we deduce that the strong magnetic shear in the vicinity of the magnetic separatrix forces all of the resonant layers in this region to lie in the so-called *diffusive-resistive* regime introduced in Ref. [26].

Finally, the thickness of a given resistive layer in p-space is $|G|^{-\nu}$ [26], so the thickness in $\hat{r}$-space is

$$\hat{\delta}_k(\hat{r}) = \frac{\tau_A^{1/2}}{\tau_R^{1/4}\,\tau_E^{1/4}\,\hat{d}_\beta^{1/2}\,(n\,|s|)^{1/2}}. \tag{108}$$

5.6 Mercier indices

The resistive layer solutions discussed in Sects. 5.4 and 5.5 are premised on the assumption that the Mercier indices at the rational surfaces, $\nu_{L\,k}$ and $\nu_{S\,k}$, take the respective values 0 and 1. As is described in Ref. [28], if this is not the case then the mismatch between the Mercier indices in the layer and those in the outer region (i.e., the region of the plasma that is governed by ideal-MHD) can be reconciled by matching the layer to the outer solution by means of an intermediate layer. However, the cylindrical expression for the Mercier interchange stability parameter takes the form

$$D_{I\,k} = -\frac{\mu_0}{B_0^2}\left[\frac{2\,(1-q^2)}{s^2}\,\hat{r}\,\frac{dp}{d\hat{r}}\right] - \frac{1}{4}, \tag{109}$$

where $p(\hat{r})$ is the total plasma pressure, and all quantities are evaluated at the rational surface [29]. Although the magnetic separatrix, $\hat{r} = 1$, is not well-described by the cylindrical approximation, if we use the previous expression to roughly gauge how $D_{I\,k}$ varies in the vicinity of the separatrix then the fact that $q \sim \ln|\hat{r}-1|$, whereas $|s| \sim 1/(|\hat{r}-1|\,\ln|\hat{r}-1|)$ [see Eqs. (34) and (77)], indicates that the strong magnetic shear in the vicinity of the separararatrix ensures that $D_{I\,k} \to -1/4$. In this case, $\nu_{L\,k} \to 0$ and $\nu_{S\,k} \to 1$ [see Eqs. (51) and (52)], and there is no need for an intermediate layer.

5.7 Plasma parameters

Suppose that the safety-factor profile is characterized by $q_0 = 1.01$, $q_{95} = 3.5$, and $q_{105} = 4.0$, as was previously assumed.

We shall adopt the model edge electron temperature and number density profiles shown in Fig. 8. These are modified hyperbolic tangent (mtanh) profiles deduced from Figs. 1 and 2 of

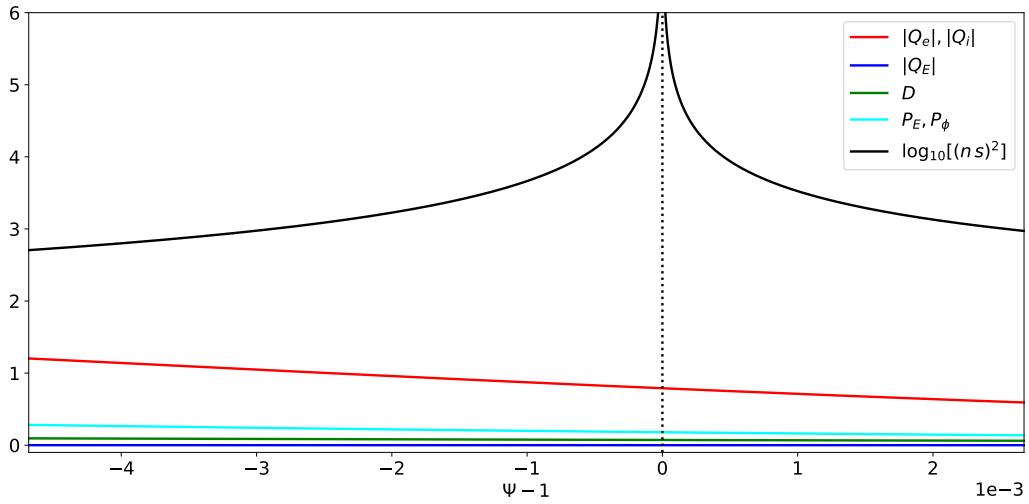

Figure 9. Normalized arameters for the resistive layers associated with an $n = 1$ RMP close to the magnetic separatrix of the JET plasma shown in Fig. 8.

Ref. [30], and represent a typical reactor-relevant high-density/low-temperature pedestal in a JET H-mode plasma (discharge 84600). We shall assume that $T_i = T_e$, for the sake of simplicity.

Let us suppose that $\omega_E + \omega_{*\,e} \simeq \omega_{*\,e}$ close to the magnetic separatrix. This is a reasonable assumption because we have no reason to imagine that the magnitude of ω_E greatly exceeds that of $\omega_{*\,e}$ in the pedestal region of an H-mode tokamak plasma. In fact, Fig. 3 of Ref. [32] suggests that the magnitude of ω_E is about a factor of 5 times smaller than that of $\omega_{*\,e}$ in the pedestal of a typical DIII-D H-mode plasma (discharge 158115).

We can complete our model by adopting the following values of the remaining unspecified plasma parameters: $B_0 = 2.0\,\mathrm{T}$, $R_0 = 2.96\,\mathrm{m}$, $a = 0.9\,\mathrm{m}$, $Z = 10.0$, $M = 2.0$, $\chi_E = \chi_\phi = 1\,\mathrm{m}^2/\mathrm{s}$ [31]. (These values are consistent with those of JET discharge 84600.) Here, M is the ion mass number, and the rather large value of Z is meant to account for the presence of a significant fraction of trapped particles, in addition to plasma impurities, close to the plasma boundary.

Figure 9 shows the normalized parameters for the resistive layers associated with an $n = 1$ RMP close to the magnetic separatrix of our example JET equilibrium. It is clear that $(n\,s)^2 \gg |Q_e|$, $|Q_i|$, $|Q_E|$, D, P_E, and P_ϕ, as was assumed in Sect. 5.5.

5.8 Overlap of resistive layers

The top panel of Fig. 10 shows the spacing (in $\hat{r}$) between successive rational surfaces $\hat{\epsilon}_k(\Psi)$, as well as the resistive layer width (in $\hat{r}$), $\hat{\delta}_k(\Psi)$, calculated in the vicinity of the magnetic separatrix for the case of an $n = 1$ RMP applied to our model JET equilibrium. It can be seen that the spacing between rational surfaces and the resistive layer width both tend to zero as the separatrix ($\Psi = 1$) is approached. However, the rational surface spacing tends to zero faster than the layer width. Consequently, the resistive layers overlap one another in the immediate vicinity of the separatrix. In fact, the region of overlap extends from $\Psi = 0.9980$ to 1.0013. Note, from the figure, that the resistive layers overlap well before either the spacing between successive rational surfaces or the layer thickness fall below the ion gyroradius (which is approximately equal to d_β).

The middle panel of Fig. 10 shows the magnitude of the layer response index, $|\Delta_k|$. It can be seen that this quantity is zero at the separatrix, but increases steeply as we move from the separatrix into the interior of the plasma, indicating that strong shielding currents are excited in the plasma interior. The steep increase is mostly due to the fact that the magnetic shear exhibits a steep decrease as we move away from the separatrix. On the other hand, the magnitude of the layer response index seems to asymptote to a constant value as we move from the separatrix into the scape-off layer (SOL) (i.e., the region $\Psi > 1$), indicating that only comparatively weak shielding currents are excited in the SOL. The magnitude of the index fails to exhibit a steep increase as we move into the SOL, despite the fact that the magnetic shear is strongly decreasing, because the electron temperature falls off rapidly with increasing distance from the separatrix. In reality, the value of $|\Delta_k|$ in the SOL is probably an overestimate, because we have not taken into account the fact that shielding current filaments in the SOL run partially through the divertor plate, which is likely to increase the effective resistivity of rational magnetic flux-surfaces in this region.

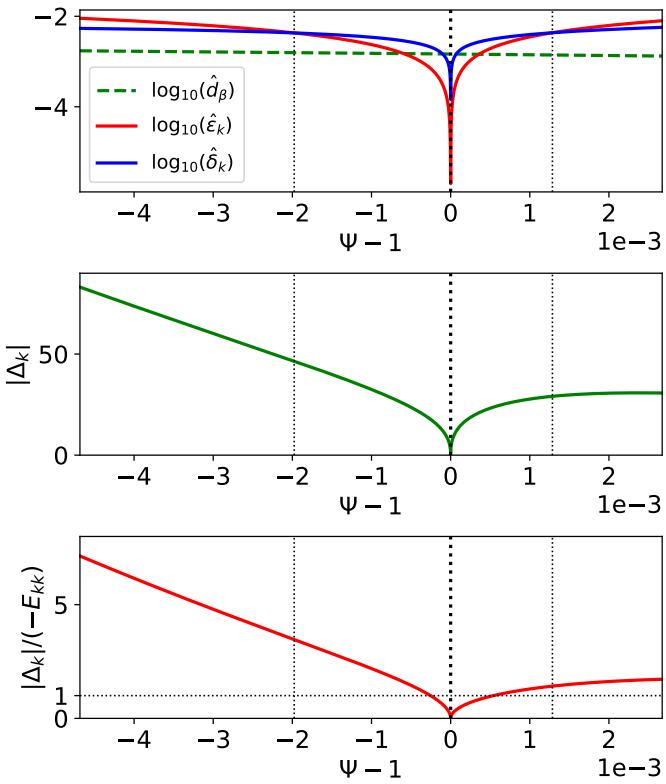

Figure 10. Overlap criterion for the resistive layers associated with an $n = 1$ RMP close to the magnetic separatrix of the JET plasma shown in Fig. 8. The bold vertical dotted lines show the location of the magnetic separatrix, whereas the faint vertical dotted lines indicate the boundaries of the region of resistive layer overlap.

The lower panel of Fig. 10 shows the ratio $|\Delta_k|/(-E_{kk})$. Here, we have used the cylindrical result $E_{kk} = -2\,|m|$ to estimate E_{kk}. It is clear that $|\Delta_k|/(-E_{kk}) \gg 1$ in the interior of the plasma. In other words, the plasma interior exhibits an ideal response to the RMP. However, $|\Delta_k|/(-E_{kk}) \lesssim 1$ in the overlap region and the SOL. In other words, it would not be unreasonable to characterize the response of the plasma in the overlap region and the SOL as being vacuum-like. Note that it is not a coincidence that the inner boundary of the overlap region corresponds approximately to the point where $|\Delta_k|/(-E_{kk}) = 1$. The plasma at the separatrix is sufficiently hot, with a typical electron temperature of 100 eV, that $|\Delta_k|/(-E_{kk})$ would greatly exceed unity were $|s| \sim \mathcal{O}(1)$. The same factor that causes the overlap of resistive layers also causes $|\Delta_k|/(-E_{kk})$ to dip below unity very close to the separatrix, and this factor is, of course, the very strong magnetic shear in the immediate vicinity of the separatrix.

Figure 11 shows analogous data to that displayed in Fig. 10 for the case of an $n = 4$ RMP. In this case, the region of resistive layer overlap extends from $\Psi = 0.9938$ to 1.0068. Thus, the width in Ψ of the overlap region exhibits a roughly linearly scaling with n. As before, the response of the plasma interior is ideal, whereas that of the overlap region and the SOL could reasonably be characterized as being vacuum-like,

5.9 Discussion

We have seen that rational surfaces accumulate in the vicinity of the magnetic separatrix. Moreover, the resistive layers, centered on the various rational surfaces, merge into one another in a very narrow region that straddles the separatrix. Furthermore, while the plasma response in the plasma interior lies in the ideal regime, that in the region of resistive layer overlap and the SOL can reasonably be modeled as being vacuum-like. It follows that the magnetic perturbation in the plasma interior is governed by Eqs. (48) and (49). In order to solve these equations, we need to know the locations of all of the rational magnetic flux-surfaces in this region, which implies that we must adopt a straight-field-line coordinate system. On the other hand, in the overlap region and the SOL, we can write $\mathbf{b} = \nabla V$, where $\nabla^2 V = 0$, which automatically ensures that the response is vacuum-like. In this case, there is no need to know the locations of the rational surfaces, which implies that it is not necessary to adopt a straight-field-line coordinate system.

We are now in a position to formulate a practical, yet physically justified, approach to

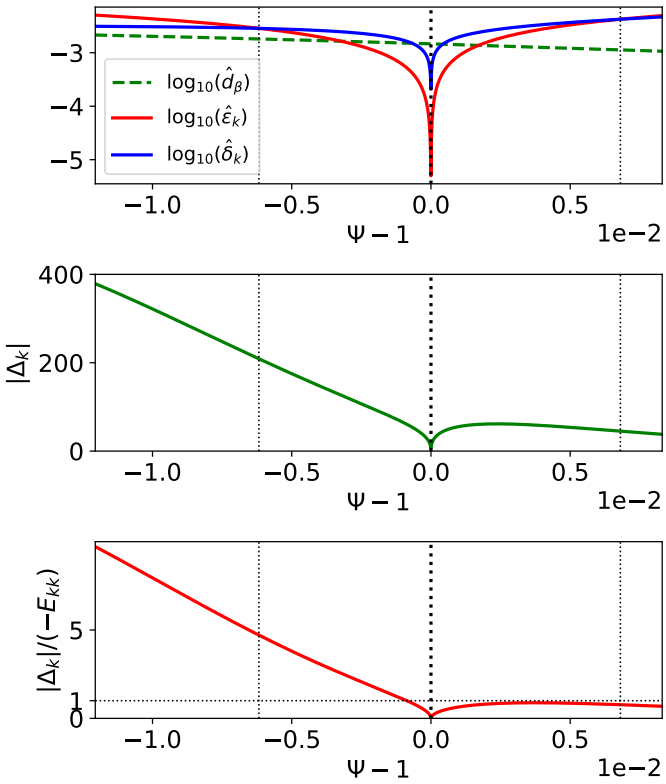

Figure 11. Overlap criterion for the resistive layers associated with an $n = 4$ RMP close to the magnetic separatrix of the JET plasma shown in Fig. 8. The bold vertical dotted lines show the location of the magnetic separatrix, whereas the faint vertical dotted lines indicate the boundaries of the region of resistive layer overlap.

calculating the response of a magnetically diverted tokamak plasma to an RMP. Let the inner boundary of the region of resistive layer overlap that straddles the magnetic separatrix lie at $\Psi = 1 - \epsilon_c$. Note that $0 < \epsilon_c \ll 1$. We must solve Eqs. (48) and (49) in the region $0 < \Psi < 1 - \epsilon_c$, using the straight-field-line coordinate system specified in Eq. (32), and treating the region $\Psi > 1 - \epsilon_c$ as a vacuum. Of course, this is the approach taken in existing plasma response codes such as GPEC [9, 11, 13, 14], in which ϵ_c is given a small positive value that is determined via an empirical guideline. (This course of action is adopted because GPEC cannot deal with the singularity of the straight-field-line coordinate system at $\Psi = 1$, and is taken in the hope that the neglect of a very narrow strip of plasma lying just inside the separatrix, as well as the plasma in the SOL, does not unduly affect the results of the calculation.) However, the analysis of this paper allows us to determine the correct value of ϵ_c from the edge plasma parameters, and also justifies the neglect of the plasma in the region $\Psi > 1 - \epsilon_c$. The fact that the region $\Psi > 1 - \epsilon_c$ is treated as a vacuum means that rational surfaces in this region do not contribute to the plasma response. In other words, the plasma response calculation only needs to take a finite, rather than an infinite, number of rational surfaces into account. Indeed, for an $n = 1$ RMP, applied to our model JET equilibrium, we only need to include rational surfaces whose resonant poloidal mode numbers are less than 8. On the other hand, for an $n = 4$ RMP, we need to include all rational surfaces whose resonant poloidal mode numbers are less than 24. Because the straight-field-line coordinate system is only required in the region $0 < \Psi < 1 - \epsilon_c$, where $\epsilon_c > 1$, the fact that the system becomes singular at $\Psi = 1$ is irrelevant. Indeed, we are free to choose a convenient non-singular coordinate system in the vacuum region, $\Psi > 1 - \epsilon_c$.

If we suppose that q_{95} is gradually increased then, at some stage, a new rational surface will enter the domain of solution, $0 < \Psi < 1 - \epsilon_c$, from the region of resistive layer overlap. Suppose that the new surface is the kth surface. The entry of the surface into the domain of solution will not cause the sudden imposition of the additional ideal constraint $\Psi_k = 0$, which would also cause a sudden change in the plasma response to the RMP [33], because $|\Delta_k|/(-E_{kk})$ is initially quite small, due to the large magnetic shear at $\Psi = 1 - \epsilon_c$. However, as q_{95} is further increased, the new surface will move into the plasma interior, where the shear is moderate, and the ideal constraint $\Psi_k = 0$ will eventually hold. In other words, ideal constraint $\Psi_k = 0$ develops gradually, as the new surface moves into the plasma interior, rather than being imposed immediately, as soon as the

Z	ϵ_c	Z	ϵ_c
1	6.86×10^{-4}	6	1.58×10^{-3}
2	9.49×10^{-4}	7	1.69×10^{-3}
3	1.15×10^{-3}	8	1.80×10^{-3}
4	1.31×10^{-3}	9	1.89×10^{-3}
5	1.45×10^{-3}	10	1.98×10^{-3}

Table 1. Variation of ϵ_c with Z for an $n=1$ RMP in a typical JET H-mode plasma.

surface enters the domain of solution.

6 Summary

In Sect. 2, we construct a simple model of a magnetically diverted tokamak plasma. We argue that the commonly used term "last closed magnetic flux-surface" (LCFS) is misleading. In fact, all equilibrium magnetic flux-surfaces are closed. However, flux-surfaces that lie outside the magnetic separatrix (i.e., the flux-surface that contains the X-point) are only partially occupied by plasma. We show that it is possible to calculate unique values of the safety-factor on flux-surfaces that lie both inside and outside the magnetic separatrix. We conclude that rational magnetic flux-surfaces exist in both regions. The safety-factor is shown to diverge logarithmically as the magnetic separatrix is approached.

A more realistic model of a magnetically diverted tokamak plasma is introduced in Sect. 3.

In Sect. 4, we show that the response of a magnetically diverted tokamak plasma to an externally generated, static, RMP can be formulated as an asymptotic matching problem. The response throughout most of the plasma is governed by the equations of linearized, marginally-stable, ideal-MHD. However, these equations are singular at the various rational surfaces in the plasma. The singularities are resolved by asymptotically matching the ideal-MHD solution to resistive layer solutions centered on the rational surfaces. The fact that the safety-factor diverges logarithmically as the magnetic separatrix is approached means that, in principle, the asymptotic matching problem involves an infinite number of coupled rational surfaces, the majority of which are located very close to the magnetic separatrix.

In Sect. 5, we examine the asymptotic matching problem close to the magnetic separatrix. We find that, due to the strong magnetic shear in the vicinity of the separatrix, both the spacing between successive rational surfaces and the resistive layer thickness tend to zero as the separatrix is approached. However, the rational surface spacing tends to zero faster. Consequently, there exits a radially thin region, that straddles the magnetic separatrix, in which the resistive layers overlap. When we calculate the response to the RMP of the resistive layers in the overlap region, as well as those in the SOL, we find that the shielding currents excited in the layers are comparatively feeble, which implies that the plasma response to the RMP in these regions is essentially vacuum-like. On the other hand, the shielding currents excited in resistive layers that lie in the interior of the plasma are comparatively strong, which implies that the plasma response to the RMP in this region is essentially ideal. We are thus able to formulate a practical, yet physically justified, approach to calculating the response of a magnetically diverted tokamak plasma to an RMP. In essence, we treat the region of the plasma that lies outside the inner boundary of the overlap region, which is situated at $\Psi = 1-\epsilon_c$, where $0<\epsilon_c\ll 1$, as a vacuum. This means that that rational surfaces that lie in the region $\Psi > 1-\epsilon_c$ do not contribute to the plasma response. Hence, a plasma response calculation only needs to take a finite number of rational surfaces into account. Our analysis enables us to determine ϵ_c from the edge plasma parameters. Assuming that the effective ion charge number takes the value $Z=10$, we find that $\epsilon_c = 2.0\times10^{-3}$ for an $n=1$ RMP, and $\epsilon_c = 6.2\times10^{-3}$ for an $n=4$ RMP, in a typical JET H-mode plasma. Table 1 shows how ϵ_c varies with Z in the former case. It can be seen that ϵ_c is a decreasing function of Z.

Funding

This research was supported by the U.S. Department of Energy, Office of Science, Office of Fusion Energy Sciences under contract DE-FG02-04ER54742.

Data availability

The digital data used in the figures in this paper can be obtained from the author upon reasonable request.

A Derivation of Induction Equation

The equilibrium magnetic field (3) can be written

$$\mathbf{B} = \mathbf{B}_p + \mathbf{B}_t = \nabla\phi \times \nabla\psi_p - q\,\nabla\theta \times \nabla\psi_p, \tag{110}$$

where $\mathbf{B}_p$ and $\mathbf{B}_t$ are the "poloidal" and "toroidal" components of the field. According to Eq. (4), the Jacobian of the ψ_p, θ, ϕ coordinate system is

$$\mathcal{J} \equiv (\nabla\psi_p \times \nabla\theta \cdot \nabla\phi)^{-1} = \frac{R_0\, q}{B_0}. \tag{111}$$

It follows that

$$B^{\psi_p} \equiv \mathbf{B}\cdot\nabla\psi_p = 0, \tag{112}$$

$$B^{\theta} \equiv \mathbf{B}\cdot\nabla\theta = \mathcal{J}^{-1}, \tag{113}$$

$$B^{\phi} \equiv \mathbf{B}\cdot\nabla\phi = \mathcal{J}^{-1}\, q. \tag{114}$$

Here, and in the following, subscripts and superscripts denote covariant and contravariant components in the ψ_p, θ, ϕ coordinate system.

The equilibrium electron fluid velocity takes the conventional form [34]

$$\mathbf{V}_e = \frac{\mathbf{E}\times\mathbf{B}}{B^2} + \frac{\nabla p_e \times \mathbf{B}}{e\, n_e\, B^2}, \tag{115}$$

where $\mathbf{E} = -\nabla\Phi$ is the equilibrium electric field, $\Phi(\psi_p)$ the equilibrium electrostatic potential, $p_e(\psi_p)$ the equilibrium electron pressure, and $n_e(\psi_p)$ the equilibrium electron number density. (Here, we are neglecting the comparatively small parallel drift velocity with respect to the perpendicular components of the fluid velocity.) It follows that

$$V_e^{\psi_p} \equiv \mathbf{V}_e\cdot\nabla\psi_p = 0, \tag{116}$$

$$V_e^{\theta} \equiv \mathbf{V}_e\cdot\nabla\theta = -\frac{(\omega_E + \omega_{*\,e})}{q}\,\frac{B_t^2}{B^2}, \tag{117}$$

$$V_e^{\phi} \equiv \mathbf{V}_e\cdot\nabla\phi = (\omega_E + \omega_{*\,e})\,\frac{B_p^2}{B^2}, \tag{118}$$

where ω_E and $\omega_{*\,e}$ are defined in Eqs. (23) and (24), respectively, and use has been made of Eq. (110).

Let $\mathbf{v}_e$ be the perturbed electron fluid velocity. Let us define the (steady-state) component of the Lagrangian electron fluid displacement that is contravariant to ψ_p such that

$$\begin{aligned} v_e^{\psi_p} = \mathbf{V}_e\cdot\nabla\xi^{\psi_p} &= \left(V_e^{\theta}\,\frac{\partial}{\partial\theta} + V_e^{\phi}\,\frac{\partial}{\partial\phi}\right)\xi^{\psi_p} = \mathrm{i}\left(m\,V_e^{\theta} - n\,V_e^{\phi}\right)\xi^{\psi_p} \\ &= -\mathrm{i}\,(\omega_E + \omega_{*\,e})\left(\frac{m\,B_t^2/q + n\,B_p^2}{B^2}\right)\xi^{\psi_p} \simeq -\mathrm{i}\,n\,(\omega_E + \omega_{*\,e})\,\xi^{\psi_p}. \end{aligned} \tag{119}$$

Here, use has been made of Eqs. (117) and (118), as well as the assumption that we are relatively close to the rational surface at which $q = m/n$.

The electron fluid equation of motion takes the form [34]

$$\frac{\nabla p_e}{e\, n_e} + \mathbf{E} + \mathbf{V}_e\times\mathbf{B} = \eta_\parallel\,\mathbf{J}, \tag{120}$$

where $\eta_\parallel$ is the parallel electrical resistivity, and $\mathbf{J}$ the current density. Note that we are neglecting the anisotropy in the plasma resistivity (as well as the thermal force), for the sake of simplicity. We are also neglecting electron inertia and electron viscosity, because the associated terms are much smaller in magnitude than the terms that we are retaining in the equation of motion. Assuming that $p_e = p_e(n_e)$, and that $\partial\mathbf{B}/\partial t = \mathbf{0}$ in a steady-state, the linearized curl of this equation, combined with Faraday's law, yields

$$\nabla\times(\mathbf{v}_e\times\mathbf{B}) + \nabla\times(\mathbf{V}_e\times\mathbf{b}) = \nabla\times(\eta_\parallel\,\mathbf{j}), \tag{121}$$

where $\mathbf{b}$ is the perturbed magnetic field, and $\mathbf{j}$ the perturbed current density. Here, we have assumed that $\nabla\cdot\mathbf{V}_e\simeq\nabla\cdot\mathbf{v}_e\simeq 0$. Now [22],

$$(\mathbf{v}_e\times\mathbf{B})_\theta = \mathcal{J}\,(v_e^\phi\,B^{\psi_p}-v_e^{\psi_p}\,B^\phi) = -q\,v_e^{\psi_p}, \tag{122}$$

$$(\mathbf{v}_e\times\mathbf{B})_\phi = \mathcal{J}\,(v_e^{\psi_p}\,B^\theta-v_e^\theta\,B^{\psi_p}) = v_e^{\psi_p}, \tag{123}$$

$$\begin{aligned}\mathcal{J}\,[\nabla\times(\mathbf{v}_e\times\mathbf{B})]^{\psi_p} &= \frac{\partial}{\partial\theta}\,(\mathbf{v}_e\times\mathbf{B})_\phi-\frac{\partial}{\partial\phi}\,(\mathbf{v}_e\times\mathbf{B})_\theta\\ &= \mathrm{i}\,(m-n\,q)\,v_e^{\psi_p} = n\,(\omega_E+\omega_{*\,e})\,(m-n\,q)\,\xi^{\psi_p},\end{aligned} \tag{124}$$

$$(\mathbf{V}_e\times\mathbf{b})_\theta = \mathcal{J}\,(V_e^\phi\,b^{\psi_p}-V_e^{\psi_p}\,b^\phi) = \mathcal{J}\,(\omega_E+\omega_{*\,e})\,\frac{B_p^2}{B^2}\,b^{\psi_p}, \tag{125}$$

$$(\mathbf{V}_e\times\mathbf{b})_\phi = \mathcal{J}\,(V_e^{\psi_p}\,b^\theta-V_e^\theta\,b^{\psi_p}) = \frac{\mathcal{J}\,(\omega_E+\omega_{*\,e})}{q}\,\frac{B_t^2}{B^2}\,b^{\psi_p}, \tag{126}$$

$$\begin{aligned}\mathcal{J}\,[\nabla\times(\mathbf{V}_e\times\mathbf{b})]^{\psi_p} &= \frac{\partial}{\partial\theta}\,(\mathbf{V}_e\times\mathbf{b})_\phi-\frac{\partial}{\partial\phi}\,(\mathbf{V}_e\times\mathbf{b})_\theta\\ &\simeq \mathrm{i}\,\mathcal{J}\,(\omega_E+\omega_{*\,e})\left(\frac{m}{q}\,\frac{B_t^2}{B^2}+n\,\frac{B_p^2}{B^2}\right)b_p^\psi \simeq \mathrm{i}\,n\,\mathcal{J}\,(\omega_E+\omega_{*\,e})\,b^{\psi_p},\end{aligned} \tag{127}$$

where use has been made of Eqs. (112)–(114) and (116)–(119), as well as the fact that B_t^2 only depends weakly on θ in a large aspect-ratio tokamak, and the assumption that $m\simeq n\,q$.

Now,

$$\mathcal{J}\,[\nabla\times(\eta_\parallel\,\mathbf{j})]^{\psi_p} = \frac{\partial}{\partial\theta}\,(\eta_\parallel\,j_\phi)-\frac{\partial}{\partial\phi}\,(\eta_\parallel\,j_\theta)\simeq\mathrm{i}\,m\,\eta_\parallel\,j_\phi, \tag{128}$$

because $|j_\theta|/|j_\phi|\simeq(a/R_0)\,(B_p/B_t)\ll 1$ in a large aspect-ratio tokamak, assuming that the perturbed current flows predominately parallel to equilibrium magnetic field-lines. Thus, the component of Eq. (121) that is contravariant to ψ_p yields

$$n\,(\omega_E+\omega_{*\,e})\left[b^{\psi_p}-\mathrm{i}\,\frac{R_0}{B_0}\left(\frac{m}{q}-n\right)\xi^{\psi_p}\right] = \frac{B_0}{R_0}\,\frac{m}{q}\,\eta_\parallel\,j_\phi, \tag{129}$$

where use has been made of Eqs. (111), (124), and (127).

References

[1] J.A. Wesson, *Tokamaks*, 4th ed., (Oxford University Press, Oxford UK, 2011).

[2] R.D. Hazeltine and J.D. Meiss, *Plasma Confinement*, (Dover, New York NY, 2003).

[3] A.H. Boozer, *Physics of magnetically confined plasmas*, Rev. Mod. Phys. **76**, 1071 (2004).

[4] Z. Chang and J.D. Callen, *Global energy confinement degradation due to macroscopic phenomena in tokamaks*, Nucl. Fusion **30**, 219 (1990).

[5] R. Fitzpatrick, *Interaction of tearing modes with external structures in cylindrical geometry (plasma)*, Nucl. Fusion **33**, 1049 (1993).

[6] N. Pomphrey and A. Reiman, *Effect of nonaxisymmetric perturbations on the structure of a tokamak poloidal divertor*, Phys. Fluids B **4**, 938 (1992).

[7] A. Reiman, *Singular surfaces in the open field line region of a diverted tokamak*, Phys. Plasmas **3**, 906 (1996).

[8] Y.Q. Liu, A. Bondeson, C.M. Fransson, B. Lennartson and C. Breitzholtz, *Feedback stabilization of nonaxisymmetric resistive wall modes in tokamaks. I. Electromagnetic model*, Phys. Plasmas **7**, 3681 (2000).

[9] J.-K. Park, A.H. Boozer and A.H. Glasser, *Computation of three-dimensional tokamak and spherical torus equilibria*, Phys. Plasmas **14**, 052110 (2007).

[10] A.H. Glasser, *The direct criterion of Newcomb for the ideal MHD stability of an axisymmetric toroidal plasma*, Phys. Plasmas **23**, 072505 (2016).

[11] J.-K. Park and N.C. Logan, *Self-consistent perturbed equilibrium with neoclassical toroidal torque in tokamaks*, Phys. Plasmas **24**, 032505 (2017).

[12] R. Fitzpatrick, *Modeling q95 windows for the suppression of edge localized modes by resonant magnetic perturbations in the DIII-D tokamak*, Phys. Plasmas **27**, 102511 (2020).

[13] Q.M. Hu, J.-K. Park, N.C. Logan, S.M. Yang, B.A. Grierson, R. Nazikian and Q. Yu, *Nonlinear two-fluid modeling of plasma response to RMPs for the ELM control in the ITER baseline*, Nucl. Fusion **61**, 106006 (2021).

[14] S. Benjamin, N.C. Logan and C. Hansen, *Computation of generalised magnetic coordinates asymptotically close to the separatrix*, Plasma Phys. Control. Fusion **67**, 065019 (2025).

[15] R.D. Hazeltine and J.D. Meiss, *Shear-Alfvén dynamics of toroidally confined plasmas*, Phys. Reports **121**, 1 (1984).

[16] S. Hamada, *Hydromagnetic equilibria and their proper coordinates*, Nucl. Fusion **2**, 23 (1962).

[17] A.H. Boozer, *Plasma equilibrium with rational magnetic surfaces*, Phys. Fluids **24**, 1999 (1981).

[18] R.C. Grimm, R.L. Dewar and J. Manickam, *Ideal MHD stability calculations in axisymmetric toroidal coordinate systems*, J. Comput. Phys. **49**, 94 (1983).

[19] R. Fitzpatrick, R.J. Hastie, T.J. Martin and C.M. Roach, *Stability of coupled tearing modes in tokamaks*, Nucl. Fusion **33**, 1533 (1993).

[20] L.J. Zheng, M.T. Kotschenreuther, F.L. Waelbroeck and M.E. Austin, *X-point effects on the ideal MHD modes in tokamaks in the description of dual-poloidal-region safety factor*, Phys. Plasmas **32**, 012501 (2025).

[21] M. Abramowitz and I.A. Stegun, *Handbook of Mathematical Functions*, (Dover, New York NY, 1964).

[22] R. Fitzpatrick, Phys. Plasmas **31**, *Calculation of tearing mode stability in an inverse aspect-ratio expanded tokamak plasma equilibrium*, 102507 (2024).

[23] R. Fitzpatrick, Phys. Plasmas **24**, *Determination of the non-ideal response of a high temperature tokamak plasma to a static external magnetic perturbation via asymptotic matching*, 072506 (2017).

[24] H.P. Furth, J. Killeen and M.N. Rosenbluth, *Finite-resistivity instabilities of a sheet pinch*, Phys. Fluids **6**, 459 (1963).

[25] C. Mercier, *A necessary condition for hydromagnetic stability of plasma with axial symmetry*, Nucl. Fusion **1**, 47 (1960).

[26] R. Fitzpatrick, *Influence of anomalous perpendicular transport on linear tearing mode dynamics in tokamak plasmas*, Phys. Plasmas **29**, 032507 (2022).

[27] A. Cole and R. Fitzpatrick, *Drift-magnetohydrodynamical model of error-field penetration in tokamak plasmas*, Phys. Plasmas **13**, 032503 (2006).

[28] R. Fitzpatrick, *Investigation of tearing mode stability near ideal stability boundaries via asymptotic matching techniques*, Phys. Plasmas **32**, 062509 (2025).

[29] A.H. Glasser, J.M. Greene and J.L. Johnson, *Resistive instabilities in a tokamak*, Phys. Fluids **19**, 567 (1976).

[30] L. Frassinetti, S. Saarelma, G. Verdoolaege, M. Groth, J.C. Hillesheim, P. Bilkova, P. Bohm, M. Dunne, R. Fridström, E. Giovannozzi, et al., *Pedestal structure, stability and scalings in JET-ILW: the EUROfusion JET-ILW pedestal database*, Nucl. Fusion **61**, 016001 (2021).

[31] Z.S. Hartwig and Y.A. Podpaly, *Magnetic Fusion Energy Formulary*, (Massachusetts Institute of Technology, Cambridge MA, 2011).

[32] R. Nazikian, C. Paz-Solden, J.D. Callen, J.S. de Grassie, D. Eldon, T.E. Evans, N.M. Ferraro, B.A. Grierson, R.J. Groebner, S.R. Haskey, et al., *Pedestal bifurcation and resonant field penetration at the threshold of edge-localized mode suppression in the DIII-D tokamak*, Phys. Rev. Lett. **114**, 105002 (2015).

[33] L.J. Zheng, M.T. Kotschenreuther and P. Valanju, *The sensitivity of tokamak magnetohydrodynamics stability on the edge equilibrium*, Phys. Plasmas **24**, 102503 (2017).

[34] R. Fitzpatrick, *Plasma Physics: An Introduction*, (CRC Press, Boca Raton FL, 2022).